Nanoscale

Accepted Manuscript

This article can be cited before page numbers have been issued, to do this please use: K. Xu, L. Yin, Y. Huang, T. A. Shifa, J. Chu, F. Wang, R. Cheng, Z. Wang and J. He, *Nanoscale*, 2016, DOI: 10.1039/C6NR05976G.

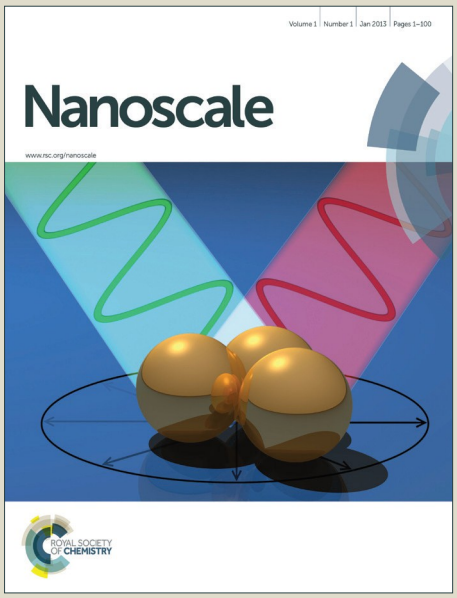

ROYAL SOCIETY OF CHEMISTRY

www.rsc.org/nanoscale

ROYAL SOCIETY OF CHEMISTRY View Article Online
DOI: 10.1039/C6NR05976G

Journal Name

ARTICLE

Synthesis, Properties and Applications of 2D Layered $M^{III}X^{VI}$ (M = Ga, In; X = S, Se, Te) Materials

Received 00th January 20xx,
Accepted 00th January 20xx

DOI: 10.1039/x0xx00000x

www.rsc.org/

Kai Xu, [a, b]† Lei Yin, [a, b]† Yun Huang,[a, b] Tofik Ahmed Shifa,[a, b] Junwei Chu,[a] Feng Wang,[a, b] Ruiqing Cheng,[a, b] Zhenxing Wang[a] and Jun He[a]*

Group III-VI compounds $M^{III}X^{VI}$ (M = Ga, In; X = S, Se, Te) are one class of important 2D layered materials and are currently attracting increasing interests due to their unique electronic, optoelectronic properties and also their great potential applications in various other fields. Similar to 2D layered transition metal dichalcogenides (TMDs), $M^{III}X^{VI}$ also own significant merits of the ultrathin thickness, ultrahigh surface-to-volume ratio, and high compatibility with flexible devices. More impressively, in contrast to TMDCs, $M^{III}X^{VI}$ demonstrate much superior properties, such as direct band gap electronic structure, high carrier mobility, rare p-type electronic behaviors, high charge density, and so on. These unique characteristics bring up high-performance device applications in electronics, optoelectronics, and optics. In this review, we aim to provide a summary on the state of the art of research activities in the 2D layered $M^{III}X^{VI}$ materials. The scope of the review covers the synthesis, properties of 2D layered $M^{III}X^{VI}$ materials and their van der Waals heterostructures. We especially focus on the applications in electronics and optoelectronics as well. Moreover, the review is concluded with some perspectives on the future developments in this field.

1. Introduction

In recent years, two-dimensional (2D) layered materials have been one of most extensively researched classes of materials.[1-14] The discovery of graphene, the monolayer counterpart of graphite, has demonstrated that it can be mechanically exfoliated from bulk graphite, and also exists stably in the atmospheres.[15-17] The essential feature of 2D layered materials is their atomic scale thicknesses. Because of the quantum confinement effect, 2D layered materials exhibit unique and fascinating physical properties and phenomena.[4, 18, 19, 20] For example, the electronic band structure of graphene exists a linear dispersion near the K point, and the charges, described as massless Dirac fermions.[21] This issue enabled scientists to come up with an abundance of new physics.[22, 23] For practical applications, compared with conventional bulk semiconductors, 2D layered semiconducting materials possess extraordinary advantages, such as atomic smoothness, dangling bond free surface, uniform and fixed thickness.[24, 25] These features intrinsically suppress thickness variation, trap generation and carrier scattering, ensuring high-performance and stable devices. Meanwhile, the atomic scale thickness of channel materials in field effect transistors (FETs) can guarantee efficient electrostatics, avoiding appearance of short channel effects.[26] On the other hand, 3D heterostructures epitaxy is limited by lattice mismatch. However, in 2D layered materials, the weak van der Waals interaction exists in two neighboring layers, and thus 2D heterostructures can be focused on band alignments rather than a lattice mismatch.[27, 28] Moreover, their planar nature is compatible with the present micormanufacturting technology and beneficial for high degree of vertical integration system.[29]

Apart from graphene, the most intensively studied 2D layered materials are transition metal dichalcogenides (TMDs), properties of which are yet distinctly complementary to that of graphene.[19, 30-33] Actually, researches based on TMDs have been continuing for decades.[33, 35-40] Now 2D thin forms of TMDs attract great scientific and engineering interest. Different from zero band gap of graphene, TMDs own a sizable band gap around 1-2 eV, great potential for FETs and optoelelctronic devices.[4, 41] Molybdenum disulfide (MoS_2) is one typical member of TMDs family, and high-performance monolayer MoS_2 top-gate FETs were first experimentally demonstrated in 2011 by Kis's group.[3] Encouraged by this, fruitful outcomes based on TMDs have been achieved, such as higher mobility engineering, lower contact resistance strategies, a stable doping technique, a large-scale MOCVD growth, ultrasensitive photodetector and flexible devices.[42-45] For example, an electron mobility of 44 $cm^2V^{-1}s^{-1}$ has been demonstrated in monolayer MoS_2 FETs at room temperature.[43] By utilizing metallic nanoparticles, experimental investigation of the doping effect on MoS_2 was studied, leading to large shift in threshold voltage.[45] Kang et al. reported 4-inch wafer-scale films of monolayer MoS_2 with excellent spatial homogeneity over the whole films.[44] The MoS_2 photodetector exhibited high responsivity of 880 AW^{-1}.[46] To date, scientists and engineers

[a] CAS Center for Excellence in Nanoscience, National Center for Nanoscience and Technology, Beijing 100190, China
[b] University of Chinese Academy of Sciences, Beijing 100049, China
†These authors contributed equally to this work.

around the world have been focusing on the practicability and commercialization of TMDs.

Similar to 2D TMDs, group III-VI compounds $M^{III}X^{VI}$ (M = Ga, In; X = S, Se, Te) are one class of important 2D layered materials and are attracting increasing interests recently.[47-55] Layered materials $M^{III}X^{VI}$ possess not only the merits of 2D layered materials discussed previously, but also additional advantages, such as higher carrier mobility, direct band gap electronic structure, rare p-type electronic behaviors, high charge density and so on.[51, 52, 56, 57] For example, the room-temperature electron mobility of InSe FETs can reach as high as 1055 $cm^2V^{-1}s^{-1}$, much larger than that of MoS_2, WSe_2, etc.[58] The InSe flakes photodetectors were broad spectra responsive from UV-visible to near infrared.[59] The photoresposivity and photodetectivity of InSe photodetectors were 10^4 AW^{-1} and 10^{13} Jones.[60] These unique characteristics and high performances motivate greatly 2D layered $M^{III}X^{VI}$ materials for practical device applications in electronics, optoelectronics, and optics in the future.

In this review, we devote to provide a summary on the state of the art in research activities of 2D layered $M^{III}X^{VI}$ materials. Initially, we will outline the crystal structure and several theoretical works based on the 2D layered $M^{III}X^{VI}$ materials and further describe the differences of electronic structure between monolayer and bulk form. Additionally, various strategies to synthesize monolayer and multilayer materials are discussed to lay the foundation for applications. Furthermore, we highlight the properties and applications of 2D layered $M^{III}X^{VI}$ materials and their van der Waals heterostructures. Finally, the review is concluded with some perspectives on the future developments in this field.

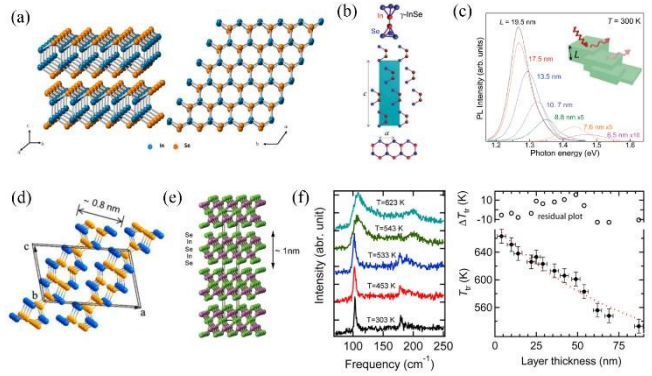

Fig. 1 (a) Side and top view of fundamental InSe crystal structures. (Reproduced with permission from ref. 62. Copyright 2014 American Chemical Society.) (b) Schematic representation of γ-rhombohedral InSe. In unit cell of γ-phase, there are three layers of Se-In-In-Se monatomic sheets along c axis. (c) PL spectra and the corresponding illustration of γ-InSe layers with various thicknesses at P = 0.1 mW, λ = 633 nm. (b-c, reproduced with permission from ref. 63. Copyright 2013 John Wiley & Sons, Inc.) (d) Layered crystal structure of GaTe, where the tellurium and gallium atoms are represented by blue and yellow spheres, respectively. (Reproduced with permission from ref. 51. Copyright 2014 American Chemical Society.) (e) Four layers of In_2Se_3. Each single layer of In_2Se_3 has a thickness of about 1 nm. (f) Left panel: Raman spectra of In_2Se_3 at different temperatures. Right panel: α→β phase transition temperature changed with thickness of In_2Se_3. (e-f, reproduced with permission from ref. 70. Copyright 2014 American Chemical Society.)

2. Crystal structure and simulations

View Article Online
DOI: 10.1039/C6NR05976G

The property and applications of materials are mainly determined by the crystal and electronic structures. It is necessary to briefly introduce the crystal and electronic structures of 2D layered $M^{III}X^{VI}$ materials in order to understand thoroughly the nature of them. According to stoichiometry, 2D layered $M^{III}X^{VI}$ materials can be classified into two main categories: MX and M_2X_3, where M stands for a transition metal from group III (M = Ga, In) and X is a chalcogen (S, Se, Te).

Figure 1a shows the schematic representation of typical MX structures. Typically, take InSe as an example, monolayer hexagonal InSe consists of planar quaternary layers, in which close-packed Se-In-In-Se monatomic sheets pile up along *c*-axis. There is strong covalent bonding within each layer. According to the stacking arrangements of quaternary layers, four polytypes are defined as *β*, *ε*, *γ*, and *δ*, which are both layered structure.[61] Among them, the *β*-phase and *γ*-phase are two common forms of InSe. For *β*-InSe, each primitive unit cell contains two quaternary layers, i.e., eight atoms. However, in unit cell of *γ*-phase, there are three layers of Se-In-In-Se monatomic sheets (twelve atoms).[61, 62] Figure 1b presents the crystal structure of *γ*-InSe with lattice parameters of c = 24.961 Å and a = 4.002 Å.[61, 63] Two adjacent layers are not connected to each other by the strong covalent bonding, but through the weak interlayer van der Waals interaction. Thus, it can be mechanically exfoliated to mono- or few-layer structures by standard scotch tape method. Bulk InSe is a typically n-type semiconductor with a direct band gap of 1.3 eV.[59, 61] Due to quantum confinement effect, photoluminescence (PL) measurement of *γ*-InSe exhibited an obvious blue-shift to higher photon energies with the decrease of thickness,[63] as illustrated in figure 1c. It is worth noting that the PL intensity is weakened with decreasing thickness, revealing layered InSe undergoes a direct-to-indirect band gap crossover. This phenomenon is in contrary to those of TMDs and other III-VI compounds. Layered GaS and GaSe own the stable hexagonal lattice structures similar to InSe, formed by stacking the fundamental S−Ga−Ga−S and Se−Ga−Ga−Se sheet building block. The thickness of single-layer GaS and GaSe are 0.75 nm and 0.8 nm, respectively.[64, 65] Moreover, the band structures of GaS and GaSe also change with their thickness.[66] In general, bulk GaS and GaSe are n- and p-type semiconductors with the indirect bandgap of 3.05 eV and 2.1 eV at room temperature.[35, 64]

Strikingly different with the relatively simple structures of GaS, GaSe, and InSe, GaTe has a more complicated crystal structure even if it is also a kind of MX stoichiometry. GaTe has a monoclinic structure, symmetry of which is less than hexagonal lattice structure, as shown in figure 1d. Two-thirds of the Ga-Ga bonds in GaTe are perpendicular to the layer and the rest are parallel to the layer.[51] Therefore, GaTe exhibits unique optical and crystallographic properties different from those of their III–VI group counterparts. In addition， bulk GaTe owns a direct band gap of about 1.7 eV at room temperature,[67] which is desirable to realize high-performance optoelectronic devices.

The most intensively studied group III–VI material with M_2X_3 stoichiometry (In_2Se_3, Ga_2Se_3 and Ga_2Te_3) is In_2Se_3. Generally, it exists in its nature with five known crystal forms (α, β, γ, δ, and κ) at various temperatures.[68, 69] The tetrahedral bonding structure underlies all of crystal forms mentioned above. There is one third of cationic vacancies in In_2Se_3 compounds where the octet rule for sp^3 hybridization is met. Among five phases, γ- and δ-In_2Se_3 are distorted wurtzite-like structure and monoclinic structure, respectively.[68] α-phase, β-phase, and recently discovered κ-phase are layered structure, formed by inserting a cationic vacancy plane every three in-layers along the *ab*-direction.[68-71] The two common forms of α-phase and β-phase have crystallographic structures that are differing in lattice parameters and material properties. Xin et al have verified that the transformation of $\alpha \rightarrow \beta$ phase is closely related to temperature.[70] Moreover, such transformation temperature is gradually increased by 130 K with the decrease of layer thickness, as shown in figure 1f. Their electrical properties also change correspondingly, which makes it to have a possible application in phase-change memories.[72] The layered crystal structure of α-In_2Se_3 is displayed in figure 1e, each single layer of In_2Se_3 are composed of a quintuple layer, in which the Se–In–Se–In–Se atomic sheets are bonded to each other through the strong covalent bonding. Therefore, the thickness of monolayer In_2Se_3 is about 1 nm,[70, 73] and the weak van der Waals interaction exists in two neighboring layers. On the basis of the *ab initio* pseudopotential total-energy method, the direct-band gap of α-In_2Se_3 is about 1.48 eV.[73] Generally, part of 2D layered $M^{III}X^{VI}$ materials are direct band gap structure, such as InSe, GaTe and In_2Se_3, benefiting for applications of high-performance optoelectronic devices.

3. Synthesis

The reliable production of high quality nanosheets is the prerequisite in order to explore their properties and possible applications. Until now, there are plenty of methods being used for the synthesis of 2D layered $M^{III}X^{VI}$ materials. Here we mainly focus on several of them and further evaluate their merits.

3.1 Chemical vapor deposition

Chemical vapor deposition (CVD) has been widely used in the growth of 2D layered materials,[55, 58, 59, 65, 72, 74-79] such as graphene, TMDs and boron nitride (BN). For instance, single-crystal hexagonal graphene with lateral size of 2 cm and wafer scale MoS_2 film were successfully synthesized by CVD method.[44, 80] The CVD growth of 2D layered $M^{III}X^{VI}$ materials has much in common with other layered materials. Figure 2a depicts the experimental setting for the growth of monolayer In_2Se_3 nanosheets.[69] In the typical process of CVD, In_2Se_3 powder was used as the only precursor and located in the middle of a tube. Silicon substrates with 285 nm thermal oxide layer served as the growth substrates, which was placed 10-15 cm away in the downstream. The optical images of the products grown in 5 and 15 minutes are illustrated in figure 2b and 2c respectively. Actually, the shape and thickness of the as-grown nanosheets could be controlled by adjusting the growth conditions, such as temperature, pressure, gas flow, substrates and so on. Analogously, ultrathin GaSe nanosheets can be synthesized with a similar experimental setting.[65] The optical and atomic force microscope (AFM) images of GaSe nanosheets are shown in figure 2d and 2e.

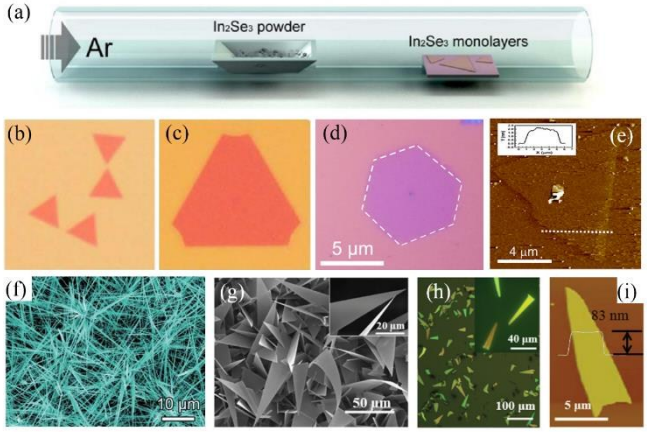

Fig. 2 (a) The schematic image of the experimental setting for In_2Se_3 nanosheets via CVD method. (b-c) Optical images of as-grown In_2Se_3 nanosheets with 5 and 15 minutes growth respectively. (a-c, reproduced with permission from ref. 69. Copyright 2015 American Chemical Society.) (d-e) Optical and AFM image of GaSe nanosheets synthesized by CVD method. (Reproduced with permission from ref. 65. Copyright 2013 American Chemical Society.) (f) SEM image of GaTe nanowires. (Reproduced with permission from ref. 74. Copyright 2014 The Royal Society of Chemistry.) (g) A typical SEM image of vertical GaTe nanosheets grown on SiO_2/Si substrate. (h) An optical image of planar GaTe nanosheets grown on mica. (i) The AFM image of a triangular GaTe nanosheet. (g-i, reproduced with permission from ref. 75. Copyright 2015 The Royal Society of Chemistry.)

Compared to sulfide and selenide, their corresponding telluride is more difficult to synthesize due to the relatively inert chemical activity. By employing gold particles as catalysts, Shen's group developed a CVD method to synthesize GaTe nanowires using gallium sheets and tellurium powders.[74] The growth temperature for GaTe nanowires is reported as 800-850 ^{0}C. Fig. 1f shows the SEM image of the as-grown nanowires. Recently, He's group successfully synthesized 2D GaTe nanosheets on rigid silicon and flexible mica.[75] Due to the different chemical environment of substrate surface, the nanosheets exhibit distinct morphology even if under exactly the same growth condition. It turns out that the chemically inert mica surface benefits the lateral epitaxy growth of GaTe nanosheets, which will be briefly discussed in the next part. The dangling bonds on the surface of SiO_2/Si substrate leads to vertical oriented nanostructures. High-quality single crystal GaTe nanosheets with lateral size of several tens of micrometers can be obtained in both case, as shown in figure 2g and 2h. Actually, to grow high-quality, large-scale and continuous 2D layered $M^{III}X^{VI}$ materials, the critical parameters must to be controlled precisely. The products of CVD are sensitive to the growth condition. The issue of controlling the stoichiometry, thickness, crystal orientation, doping, defects, domain size and large scale is the subject of future experimental effort to realize high quality 2D layered $M^{III}X^{VI}$ materials.

3.2 Van der Waals epitaxy

Due to week van der Waals (vdW) interaction existing naturally in two neighboring layers, vdW epitaxy is an ideal approach for growth of 2D layered materials. Especially, 3D heterostructures epitaxy in group III-IV compounds is limited by lattice mismatch. However, 2D heterostructures based on layered materials can be focused with respect to band gap alignments rather other lattice mismatch. One requirement for vdW epitaxy growth is that the surface of the substrate should be chemically inert (free of surface dangling bonds). The common substrates for this method include mica, graphene, BN and so on. Since the associated energy of vdW force (40-70 meV) is much smaller than that of covalent bonding energy (200-6000 meV), epitaxial heterostructure is attainable even if the lattice mismatch is significant between materials.[81]

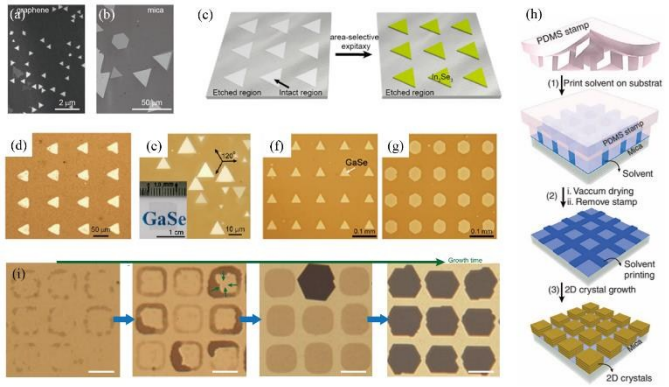

Fig. 3 (a-b) SEM image of In_2Se_3 flakes grown on graphene and mica respectively. (c) Schematic image illustrates the selective-area growth of In_2Se_3 via oxygen plasma etching. (d) Optical image of patterned In_2Se_3 flakes grown on modified mica. (a-d, reproduced with permission from ref. 76. Copyright 2013 American Chemical Society.) (e) Optical image of GaSe nanosheets grown on mica. (f-g) Optical image of GaSe arrays by site-selected growth. (e-g, reproduced with permission from ref. 85. Copyright 2014 American Chemical Society.) (h) Schematic image illustrating the process of microintaglio printing. (i) The optical image of Bi_2Se_3 crystals grown on mica at different stages. (h-i, reproduced with permission from ref. 55. Copyright 2015 Macmillan Publishers Limited.)

It is worth mentioning that, in order to realize the integration of electronic and optoelectronic devices, achieving large-area as well as patterned growth of 2D materials is essential.[82-84] VdW epitaxy growth combined with surface treatment technique has been developed to reach this goal.[76, 85] The purpose of surface treatment is to control the nucleation site. So far, oxygen plasma etching and microintaglio printing have been utilized to efficiently define the nucleation sites of GaSe and In_2Se_3 nanosheets on mica. As shown in figure 3a, 3b and 3e, the location of In_2Se_3, GaSe nanosheets grown on the surface of graphene or mica are random.[76, 85] However, after selective oxygen plasma etching, nanosheets would only nucleate at regions without etching, resulting in patterned In_2Se_3 and GaSe nanosheets as illustrated in figure 3d, 3f and 3g. Another method to control the nucleation sites is microintaglio printing.[55] The process of this method is schematically illustrated in figure 3h. Polydimethylsilocane (PDMS) with designed structures was prepared in advance through a standard photolithography and replica moulding process.[55] Solvent ink made of PDMS oligomer dissolving in acetone, ethanol and cyclohexane was then dropped on the surface of the prepared PDMS stamp. Freshly cleaved mica sheet was placed face-to-face with the PDMS stamp. Then, the imprints were left on the non-contacted region and the treated mica was immediately used for the growth of 2D materials. In situ observation indicated that Bi_2Se_3 nanosheets preferred to nucleate at the edge of additional residue aggregations and further expanded to the region without ink residues. As the growth time increases, the nuclei would eventually coalesce to cover the whole region contacted with PDMS stamp. This process is shown in figure 3i. The techniques based on vdW epitaxy and surface etching can realize the large-scale pattern of 2D layered $M^{III}X^{VI}$ materials, providing a groundwork for next-generation electronic and optoelectronic devices.

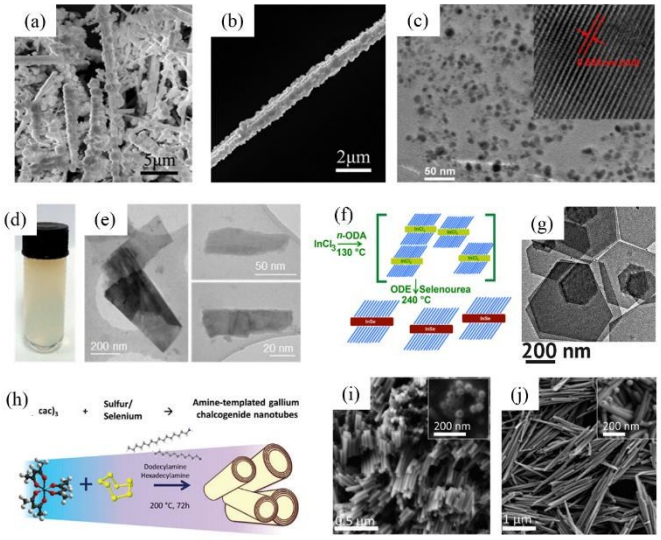

Fig. 4 The SEM image of (a) 1D In_2Te_3 nanostructures and (b) a single 1D In_2Te_3 nanostructure grown by solvothermal method. (Reproduced with permission from ref. 79. Copyright 2012 American Chemical Society.) (c) TEM image of Ga_2S_3 nanoparticles synthesized by solvothermal method. (Reproduced with permission from ref. 87. Copyright 2014 Trans Tech Publications Ltd.) (d) Optical image of a typical GaS powder dispersion in 2-propanol. (e) Representative TEM image of GaS flakes exfoliated in IPA (c-e, reproduced with permission from ref. 44. Copyright 2015 American Chemical Society). (f) Scheme of InSe nanosheets grown by ligand-templated method. (g) Corresponding TEM image of as grown InSe nanosheets. (f-g, reproduced with permission from ref. 90. Copyright 2016 American Chemical Society.) (h) Scheme and (i-j) SEM micrograph of GaS and GaSe nanotubes grown by long-chain amine-templated method. (Reproduced with permission from ref. 91. Copyright 2016 The Royal Society of Chemistry.)

3.3 Solution-phase method

Apart from vapor phase deposition, solution-phase methods, including solvothermal, liquid exfoliation, ligand-templated growth and so on, are able to synthesize $M^{III}X^{VI}$ materials with large scale.[87-91] Various kinds of nanostructures can be synthesized by solvothermal method. As an example, In_2Te_3 nanowires were prepared and applied to broad spectral photodetecotrs.[79] The morphology of synthesized nanowires is

shown in figure 4a and 4b. Electron dispersive X-ray (EDX) and X-ray diffraction (XRD) results further demonstrate the synthesized nanostructures are In_2Te_3. Ga_2Se_3 nanoparticles could also be synthesized using solvothermal method at room temperature.[87] Unlike the method of synthesizing In_2Te_3, this kind of reaction takes place in a round bottomed flask without organic solvents. Instead, aqueous solution of gallium (III) chloride and sodium thiosulphate are the only precursors. High resolution transmission electron microscope (HRTEM) image of synthesized Ga_2Se_3 nanoparticles is shown in figure 4c. The size of the synthesized nanoparticles can vary from 12 nm to 35 nm.

Over the past few years, liquid exfoliation is well developed for its versatility and prolificacy, as well as its simple preparation process. Typically, high-yield thin layer 2D layered materials can be obtained by ultrasonication in proper solvents. The products are usually a few hundred of nanometers in size and 1 to 10 layers thick. Benefiting from the adsorption of molecules from solution, the flakes are relatively stable against re-aggregation.[92] Until now, liquid exfoliation has been widely applied for the production of various 2D layered materials. However, its application for synthesis of $M^{III}X^{VI}$ materials is just at the beginning. Coleman's group demonstrated the effective production of GaS nanosheets by sonicating GaS powder in isopropanol.[88] The typical dispersion is shown in figure 4d and the transmission electron microscope (TEM) images of obtained GaS nanosheets are shown in figure 4e. The statistical results indicate that the products vary from each other in the range of 3-80 layers thick and 50-1000 nm large, which could be further selected by controlling the centrifugation parameters. This method could also be used for the preparation of hybrid nanocomposites.[89]

Furthermore, ligand-templated growth is another alternative to synthesize nanomaterials with different structures. Besides, it offers additional advantages to synthesize 2D nanosheets even if the intrinsic vdW interaction is lacking. For instance, PbS, CdSe, ZnS, CuS nanosheets have been successfully obtained through this method.[93-95] It usually began with the formation of a ligand template and then followed by a sulfurization/selenization process. Recently, GaS/GaS nanotubes and ultrathin InSe nanosheets were achieved by this method.[90, 91] The schematics of related process are depicted in figure 3f and 3h. To synthesize InSe nanosheets, indium chloride and octadecylamine (ODA) are firstly mixed to form an indium-ODA complex and then reacted with selenourea dissolved in 1-octadecene (ODE).[90] It is worth mentioning that the ODA served as an essential template ligand for the formation of InSe nanosheets during this process. The as-grown nanosheets shaped as regular hexagon (as shown in figure 4g), whose lateral size could be 800 nm and thickness be 5 nm. Due to the distinct properties of template ligands, flexible nanostructures could be fabricated via the ligand-templated growth. Nicolosi's group developed a method to grow gallium sulfide/selenide nanotubes under the direction of long-chain amines.[91] In their recipe, gallium acetylacetonate and sulfur/selenium were chosen as the precursors and also hexadecylamine and dodecylamine were chosen as the solvents as well as the directing template. The images of as-synthesized GaS and GaSe nanotubes are illustrated in figure 4i and 4j.

3.4 Other methods

Due to the weak vdW interactions between adjacent layers, single or few layer 2D materials can be easily obtained by micromechanical cleavage using adhesive tape. Without reacting or contacting with other chemical reagents, the obtained thin layer nanosheets own clean surfaces and high-quality crystal structures, which are ideal for exploring electronic, optoelectronic applications as well as fundamental research. In a typical process, high quality bulk counterparts (usually synthesized by Bridgman method) were thinned by repeatedly folding the adhesive tape. After scraping, the thinned sheets were transferred onto the surface of rigid substrates. Their thickness can be confirmed with the help of AFM, Raman, HRTEM or other characterization methods. Some other methods were also successfully developed to synthesize large-area $M^{III}X^{VI}$ films.[57, 96] For instance, Elam's group used hexakis (dimethylamido) digallium ($Ga_2(NMe_2)_6$, where Me=CH_3) and hydrogen sulfide (H_2S) to deposit GaS_x films by atomic layer deposition and demonstrated its potential applications for lithium-ion battery anode.[96] Geohegan's group presented a pulsed laser deposition method to rapidly grow uniform GaSe nanosheets with digital thickness control.[57] Aydoğan's group realized the electrochemical deposition of GaTe thin films on p-type Si substrate and studied the temperature related current-voltage characteristics of Si/GaTe diode.[97] It is reasonable to predict that high-quality $M^{III}X^{VI}$ materials with desired properties can be prepared using improved methods in the future.

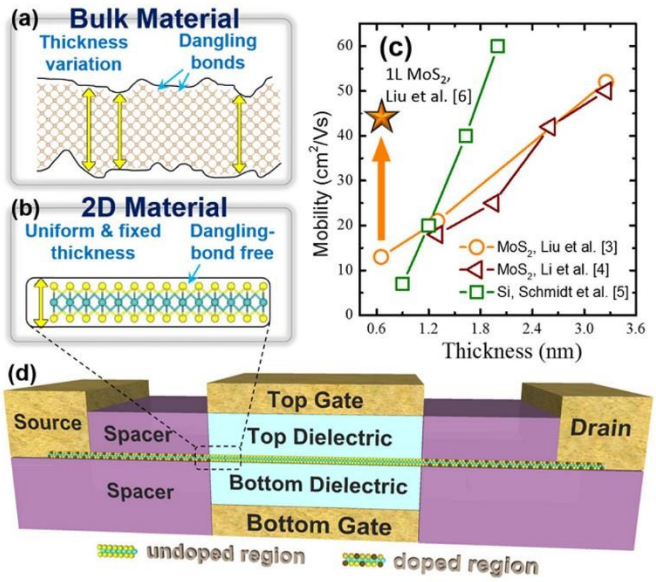

Fig. 5 (a) Issues of bulk materials and (b) advantage of 2D layered materials. (c) Silicon suffers from a more serious degeneration of mobility, compared with 2D materials. (d) Schematic of a 2D FETs. (Reproduced with permission from ref. 26. Copyright 2015 Institute of Electrical and Electronics Engineers.)

4. Properties and applications

4.1 Electronics

In the past 60 years, the introduction of high-performance boosters such as high-*k* dielectrics, metal gate, strain and new geometries have improved the performance of transistor.[98] With shrinking of the dimensions of planar devices, especially in bulk planar devices, good electrostatic control of the channel by the gate voltage is required. However, thin gate oxides result in increased leakage, high substrate doping and mobility degradation. The International Technology Roadmap for Semiconductors (ITRS) has predicted additional new materials and new transistor geometries will be needed to resolve the current challenges of transistor scaling in the next 10 years.

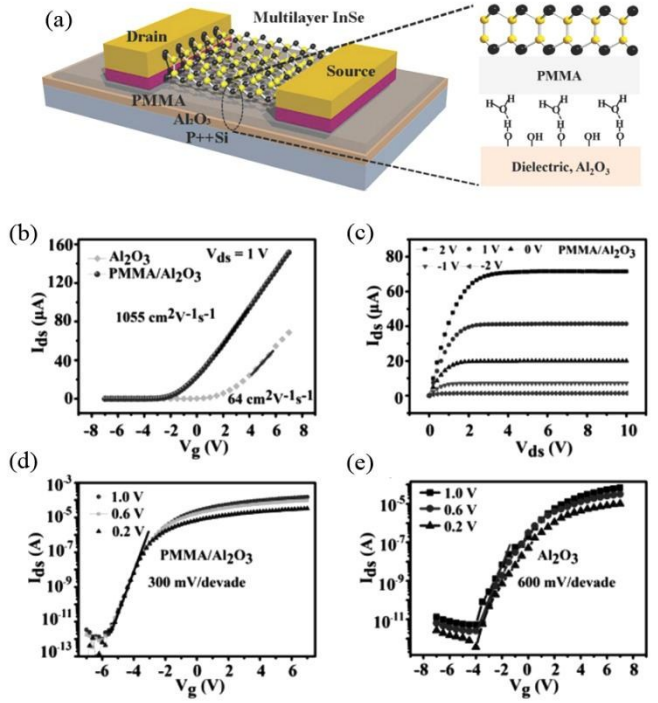

Fig. 6 (a) The PMMA/Al_2O_3 double layer is chosen as dielectric, and the PMMA can screen the interfacial Coulomb scattering, such as hydroxyl groups, water and chemical absorptions. (b) Transfer and (c) output characterization of multilayer InSe FETs with PMMA/Al_2O_3 dielectric layer. (d) The calcualted SS of multilayer InSe FETs with PMMA/Al_2O_3 dielectrics is 300 mV and on/off ratio is 10^8 $cm^2V^{-1}s^{-1}$, also higher than that of multilayer MoS_2 FETs. (e) Transfer characteristics of InSe FETs fabricated on Al_2O_3 dielectric. (Reproduced with permission from ref. 58. Copyright 2014 John Wiley & Sons, Inc.)

2D layered semiconducting materials are highly promising as channel materials for the ability to control the channel thickness at atomic level.[3] This feature can improve the gate control over the channel and suppress short channel effects,[99] and meanwhile, their planar nature is more compatible with present fabrication technology and beneficial for high degree of vertical integration system.[100] As schematically shown in Figure 5a and 5b, although conventional materials, such silicon and germanium, can also be reduced to very thin layer, the atomically smooth and dangling bond-free surface of 2D materials intrinsically suppress the interface state density and surface roughness scattering, guaranteeing robust devices performance. Thus, silicon suffers from a more serious degeneration of mobility, compared with 2D materials, as presented in Figure 5c. Moreover, the mobility of 2D materials can be further enhanced with improvement of the material quality and gate dielectric engineering.[43, 101-103] The discovery of graphene has paved the way to rediscovery of other 2D materials, such as TMDs, BN, $M^{III}X^{VI}$ and black phosphorous. 2D layered semiconductors own the advantage over graphene of extended bandgap tunability through thickness, composition, and strain.

So far, many studies based on 2D layered materials have been conducted in FETs, which are the central building element for logic circuit.[3, 104, 105] These materials used in FETs as transport channel, mainly focus on TMDs such as MoS_2 and WSe_2.[3, 5, 106-108] However, actually, it is reported that MoS_2 is not desirable materials as channel because of low temperature mobility (0.1-200 $cm^2V^{-1}s^{-1}$) and heavy electron effective mass ($m^* = 0.45m_0$).[105, 109] Indium selenide (InSe), being a typical layered material, belonging to group III-IV compounds has two common forms of InSe are the *β*-phase and *γ*-phase. The structure of InSe has been presented in previous part. Importantly, InSe owns lower electron effective mass ($m^* = 0.145m_0$) and exhibits a very high mobility (10^3 $cm^2V^{-1}s^{-1}$), which make it possess a great potential layered material for high-performance electronic devices.[56, 58, 110, 111] In the view of the devices, the real mobility easily suffers from various scatterings, especially which comes from the interface of dielectric/2D materials.[58, 112] For example, interfacial Coulomb impurities, surface roughness and surface polar phonon significantly decrease the mobility of devices.[113] Especially with thickness of materials decreasing to a few nanometers, the interfacial Coulomb impurities become dominant scattering factor because of the shorter distance of impurities and electrons in monolayer materials.[58] Traditional dielectric layers such as SiO_2, Al_2O_3, HfS_2 etc., have lots of hydroxyl groups and other trap states at the interface between dielectric and channel, which leads to various interface scattering. Thus, the mobility of devices can be enhanced by suppressing and eliminating these scattering from interface. As shown in Figure 6a, the PMMA/Al_2O_3 double layer is chosen as dielectric, and the PMMA can screen the interfacial Coulomb scattering, such as hydroxyl groups, water and chemical absorptions. Figure 6b and 6c manifest the transfer and output characterization of multilayer InSe FETs with PMMA/Al_2O_3 dielectric layer. The field-effect mobility of devices can be estimated from the transfer characterization by the following equation: $\mu = Lg_m/WC_iV_{ds}$, where L is the channel length, g_m is the transconductance extracted from the transfer characteristics, W is the channel width, C_i is the capacitance, and V_{ds} is the drain voltage.[114] In the case of PMMA/Al_2O_3, the mobility was found to be as high as 1055 $cm^2V^{-1}s^{-1}$, larger than the mobility (64 $cm^2V^{-1}s^{-1}$) of FETs with Al_2O_3. Moreover, this valve was much higher than that of MoS_2, WSe_2, etc., and even can be comparable to that of strained 25 nm Si thin-film. The improvement of performance from PMMA/Al_2O_3 dielectric to Al_2O_3 dielectric was attributed to the suppression of interface Coulomb scattering. On the other hand, the subthreshold swing

(SS) and on/off ratio of current in FETs is extremely important, because it implies a remarkably large on/off ratio at a small supply voltage.[115] The SS can be calculated by the following eqution: SS = $dV_g/d(\log I_d)$.[116] Figure 6d presents that the calcualted SS of multilayer InSe FETs with PMMA/Al_2O_3 dielectrics is 300 mV and on/off ratio is 10^8 $cm^2V^{-1}s^{-1}$, also higher than that of multilayer MoS_2 FETs. The I_d-V_d curve shows a linear regime under low voltage and a current saturation regime at high voltage, which agrees with characteristics of conventional NMOS transistors and are beneficial for practical applications.

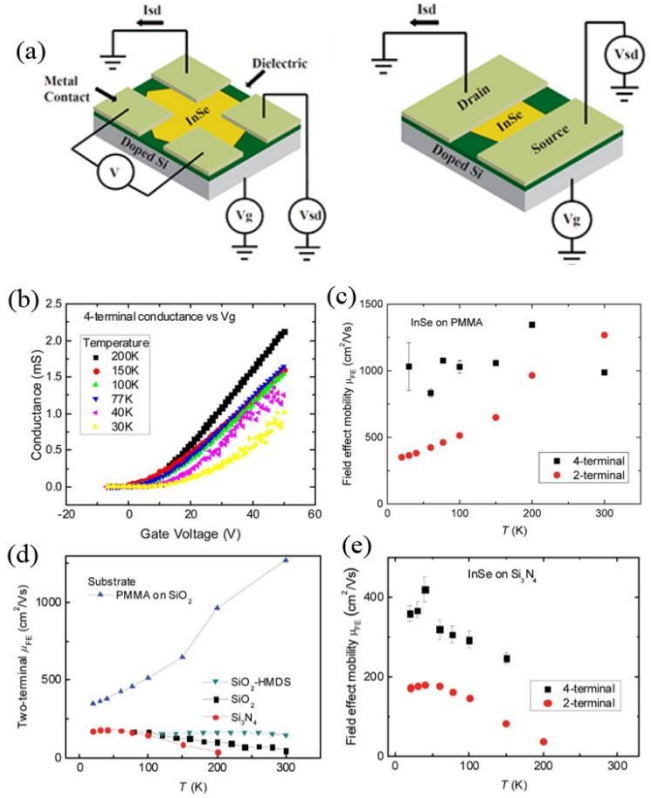

Fig. 7 (a) Schematically the two-terminal and four-terminal measurements. (b) Four-terminal conductance of InSe FETs on PMMA/SiO_2 at different temperature. (c) Comparison between the field effect moblity of two- and four-terminal measurements. (d) Comparison between the field effect moblity of two-terminal measurements at different substracts. (e) Comparison between the field effect moblity of two and four terminal measurements at Si_3N_4. (Reproduced with permission from ref. 56. Copyright 2015 American Chemical Society.)

Although the room-temperature mobility of multilayer InSe FETs with PMMA/Al_2O_3 dielectrics can reach 1000 $cm^2V^{-1}s^{-1}$, the intrinsic and temperature-dependent mobility of InSe in the two dimensional scales is not yet clearly eleborated, because of the limit of two-terminal measurement. Sukrit et al. excluded the effect of contact, temperature, and different substrate dielectric and obtained the intrinsic transport properties and mobility by four-terminal measurement.[56] Figure 7a illustrates schematically the two-terminal and four-terminal measurements. The transfer curve of multilayer InSe FETs fabricated on PMMA substrate and the temperature-dependent mobility of two different measurements are obtained, as shown in Figure 7b and 7c. With the decreasing of temperature, the mobility measured by two-terminal method degrades largely from 1250 $cm^2V^{-1}s^{-1}$ to 300 $cm^2V^{-1}s^{-1}$, while four-terminal field effect mobility displays weak temperature dependence. The phenomenon results from the impact of worsened contacts at low temperature.[43] Furthermore, the different substrates such as SiO_2, Si_3N_4, and HMDS-modified SiO_2 are utilized as presented in Figure 7c, which indeed confirmed PMMA as dielectric of FETs are supervisor than other substrates. As discussed above, the mobility of InSe FETs fabricated with PMMA exhibited a rapid degradation with temperature decreases and the mobilities of other substrates display opposite trend of temperature dependence. Thus, it suggested PMMA does have the advantage of high mobility than conventional dielectrics, despite its being somehow unstable against temperature cycling.

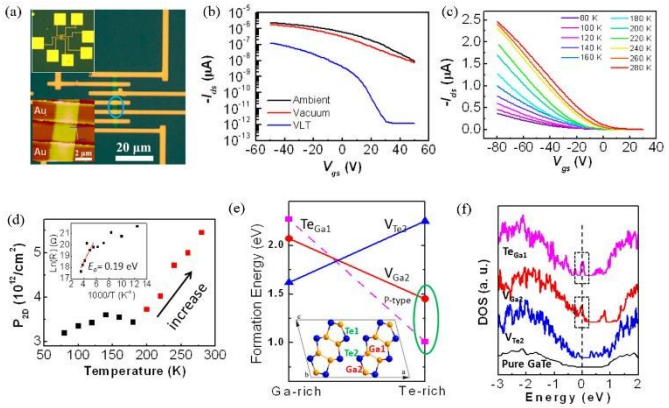

Fig. 8 (a) The FETs based on multilayer GaTe nanosheets were fabricated on SiO_2 substrate. (b) The transfer characteristics of GaTe FETs were strongly affected by the environments. With temperature decreasing, the electrical properties were further enhanced. (c) The transfer characteristics at various temperature. As temperature increased, V_{th} of FETs shifted to the direction of positive voltage, indicating more carriers are generated in GaTe channel. (d) The 2D channel density was extracted from the various-temperature transfer curve. (e) Three low-energy native defects as a function of the Te chemical potential and (f) their corresponding electronic structures. (Reproduced with permission from ref. 51. Copyright 2015 American Chemical Society.)

Encouraged by the achievements in InSe, various other layered group III-IV compounds such as GaS, GaSe, GaTe and In_2Se_3, have been studied.[47, 51, 52, 117] The FETs based on multilayer GaTe nanosheets were fabricated on SiO_2 substrate, and the electric properties were measured as shown in Figure 8. The transfer characteristics of GaTe FETs were strongly affected by the environments. With temperature decreasing, the electrical properties were further enhanced. The off state current of the device reduced to pA magnitude, and the on/off ratio raised to 10^5 which is enhanced more than 400 times, as indicated in figure 8b. To better understand the mechanism as to how the temperature affected the electric properties of GaTe FETs, various temperature measurements and theoretical simulations were conducted. As temperature increased, V_{th} of FETs shifted to the direction of positive voltage, indicating more carriers are generated in GaTe channel. Furthermore, the 2D channel density was extracted from the various-temperature transfer curve, as displayed in Figure 8d. Below temperature of

200 K, the carrier density increases slightly, while above 200 K, it increased sharply. This phenomenon indicated that some defect states were thermally activated above 200 K and the activation energy was extracted to be 0.19 eV. First-principles calculation also confirmed this result. Figure 8e and 8f illustrate three low-energy native defects as a function of the Te chemical potential and their corresponding electronic structures. It implied that Ga vacancy and the Te-on-Ga antisite had the lower formation energy, but the activation energy of Te-on-Ga antisite was 0.6 eV and can be excluded.[118] Thus, the activated behavior was attributed to Ga vacancy and this finding were of significance to understand the physical nature of GaTe FETs and unlocked the hurdle for practical application of FETs based on group III-IV compounds.

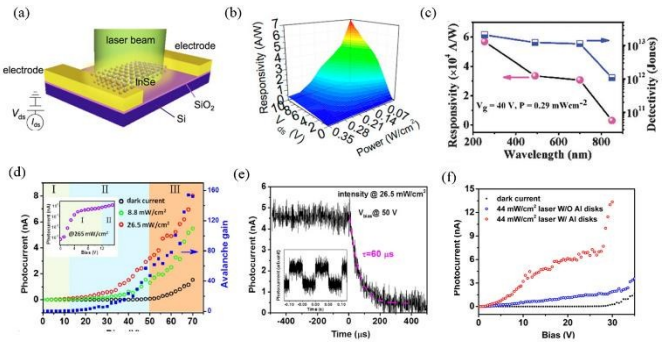

Fig. 9 (a) The InSe flakes can be excited in the technological important near-infrared spectra range at room temperature, which provides more opportunities for planar device architectures and near-infrared light sensing. Few-layered InSe photodetectors were fabricated on SiO_2/Si substrate. (b) The photoresponsivity can be tuned by drain voltage. Larger drain voltage reduces the transit time and recombination rate and thus enhances the photoresponsivity of photodetector. (Reproduced with permission from ref. 59. Copyright 2015 American Chemical Society.) (c) The responsivity and detectivity as a function of illumination wavelengths with light intensity 0.29 mW/cm^{-2} at the gate voltage 40 V. (Reproduced with permission from ref. 60. Copyright 2015 The Royal Society of Chemistry.) (d) By utilizing the avalanche effect, the performance of InSe photodetectors were enhanced largely, with improved photoresponsivity, low dark currents and (e) fast response time. The external quantum efficiency of 334% and high avalanche gain of 47 were achieved. (f) Plasmonic Al disk nanoantennas patterned on the InSe flaks can improve the light absorption. (Reproduced with permission from ref. 134. Copyright 2015 American Chemical Society.)

4.2 Optoelectronics

The conversion between light and electric signal is an extremely significant technology that affect our daily life. In recent years, 2D layered materials have emerged and rapidly established themselves for next-generation ultrathin and flexible optoelectronic devices.[46, 105, 119-125] 2D layered materials can be compatible with the highly silicon-based platform for optoelectronics, leading to large-scale integration into optoelectronic circuits.[126] Graphene, as the first member of 2D layered materials family, is an exciting material which has been explored for developing photodetector.[127] However, the intrinsically weak light absorption (2.3%) and high dark current limit the practical applications of graphene. Other 2D layered materials beyond graphene, are complementary to the properties of graphene. The relatively high earth abundance of group III-IV compounds and their direct band gaps in the visible range render them as light-absorption material.[128] Moreover, compared with conventional direct band gap semiconductor, they own additional properties of transparency, mechanical flexibility and easy processing characteristics.

Another feature in 2D layered materials is strong quantum confinement effects.[4, 63, 129] Figure 1c depicts the PL spectra of InSe flakes with different thicknesses. With thickness decreasing, the near-band gap PL peak exhibits a strong blue shift with 200 meV. Meanwhile, the peak intensity drops significantly, as thickness is below 10 nm. The quantum confinement effects observed in InSe flakes were stronger than that of MoS_2 and also lead to a crossover from direct bandgap to indirect bandgap when the thickness of InSe flakes lower than 5 nm. The InSe flakes can be excited in the technological important near-infrared spectra range at room temperature, which provides more opportunities for planar device architectures and near-infrared light sensing. Few-layered InSe photodetectors were fabricated on SiO_2/Si substrate, excited at 633 nm, as shown in Figure 9a. Photoresponsivity of the photodetector implies the capacity of optoelectric conversion and can be defined as the ratio of the generated photocurrent I_{ps} to optical power density P irradiating on the detector ($R = I_p/PS$).[127, 130] Figure 9b illustrates the photoresponsivity can be tuned by drain voltage. Larger drain voltage reduces the transit time and recombination rate and thus enhances the photoresponsivity of photodetector. On the other hand, detectivity indicates the capacity of detection for weak optical signals and is estimated by the equation $D^* = RS^{1/2}/(2qI_d)^{1/2}$, where I_d is the dark current. The responsivity and detectivity as a function of illumination wavelengths with light intensity 0.29 mW/cm^{-2} at the gate voltage 40 V are presented in Figure 9c. The responsivity and detectivity are as high as 10^4 AW^{-1} and 10^{14} Jones respectively. The InSe flakes photodetectors are broad spectra responsive from UV-visible to near infrared. Moreover, the photoresponsivity and photodetectivity of InSe photoresponse are superior to those of the most other 2D materials, commercial Si and InGaAs photodetectors.[131-133]

Actually, for photodetector, the responsivity and detectivity are not the only factors that be considered because the amplification circuit can be used to improve them. However, the signal-to-noise ratio (S/N) and response time cannot be tuned by the signal process, which are problematic in practical applications. Lei et al. designed and demonstrated an avalanche InSe photodetector.[134] By utilizing the avalanche effect, the performance of InSe photodetectors were enhanced largely, with improved photoresponsivity, low dark currents and fast response time. The avalanche effect of InSe-based photodetector was realized by large Schottky barrier between metal Al and semiconductor InSe. This device contained two Schottky junctions that are back to back. Because of the reverse biased Schottky barriers, the dark currents were suppressed dramatically. The external quantum efficiency of 334% and high avalanche gain of 47 were achieved, as shown in Figure 9d. Concurrently, an ultrafast response time of 60 μs was achieved, which was better than most reported 2D layered materials. Furthermore, the avalanche effect leaded to photocarriers

utilized more efficiently, but the number of photocarriers was not enhanced. A recent work has demonstrated that plasmonic Al disk nanoantennas patterned on the InSe flaks can improve the light absorption, as presented in Figure 9f. It is clearly indicated that the plasmonic enhancement lead to large photocurrent. The combination of the avalanche effect and plasmonic effect can work together and similar strategies can also be used in other 2D materials based photodetectors.

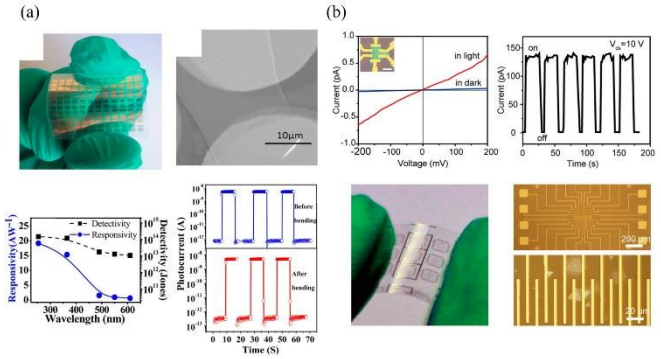

Fig. 10 (a) GaS nanosheets photodetector fabricated on flexible PET substrates. Ultrahigh detectivity at different wavelengths was calculated in the range of 10^{12}-10^{13} Jones for visible light and about 10^{14} Jones for ultraviolet light. (Reproduced with permission from ref. 48. Copyright 2015 American Chemical Society.) (b) GaSe nanosheets synthesized by a facile vdW epitaxy method also exhibited excellent photoresponse on flexible and transparent mica substrates, regardless of repeated bending. (Reproduced with permission from ref. 85. Copyright 2015 American Chemical Society.)

2D layered materials are easily compatible with current micormanufacturting techniques. Meanwhile, their large surface-to-volume ratio and low dimensional features show higher light sensitivity than bulk materials. Moreover, 2D layered materials also exhibit excellent mechanical properties, which make them to be utilized in flexible optoelelctronics. Flexible devices greatly benefit from the development of 2D layered materials, which are accessible on soft polymeric or plastic substrates. Figure 10a shows GaS nanosheets photodetector fabricated on flexible PET substrates. Ultrahigh detectivity at different wavelengths was calculated in the range of 10^{12}-10^{13} Jones for visible light and about 10^{14} Jones for ultraviolet light. The stability of the GaS nanosheets photodetector on PET substrates was measured before/after bending. The on/off ratio of photocurrent is 10^4 after bending, showing highly responsive and stable. On the other hand, GaSe nanosheets synthesized by a facile vdW epitaxy method also exhibited excellent photoresponse on flexible and transparent mica substrates, regardless of repeated bending, as shown in Figure 10b. Thus, planar feature, mechanical stability, high photoresponse and compatible manufacturing techniques make layered $M^{III}X^{VI}$ materials own great potential for flexible optoelectronics in the future.

Patterning 2D layered materials has a benefit for integration of electronic optoelectronic devices. As discussed in Figure 3, Zheng et al. has patterned large-area arrays of In_2Se_3 on transparent mica substrate.[55] In_2Se_3 is another important n type semiconductor with direct bandgap of 1.3 eV and exhibited great photoresponsivity and fast response time.[135] Figure 11 shows the photoresponse of patterned and packaged In_2Se_3 photodetectors. The photocurrents from single and multiple devices exhibited excellent, stable and cooperative response, as presented in Figure 11c. The In_2Se_3 photodetector arrays showed ultrahigh responsivity of 1650 AW^{-1} at low incident power P = 622 $nWcm^{-2}$. Moreover, dozens of devices were fabricated and all has proved excellent photoresponse, indicating the uniformity of this photodetector arrays. For practical applications of optoelectronic devices, packaging is important aspect. Figure 11g shows packaged In_2Se_3 photodetectors arrays, which exhibit remarkable flexible and mechanical durability, with little change even after repeated dynamic bending tests. The patterned and packaged In_2Se_3 photodetectors hold a great promise for next-generation photodetector arrays.

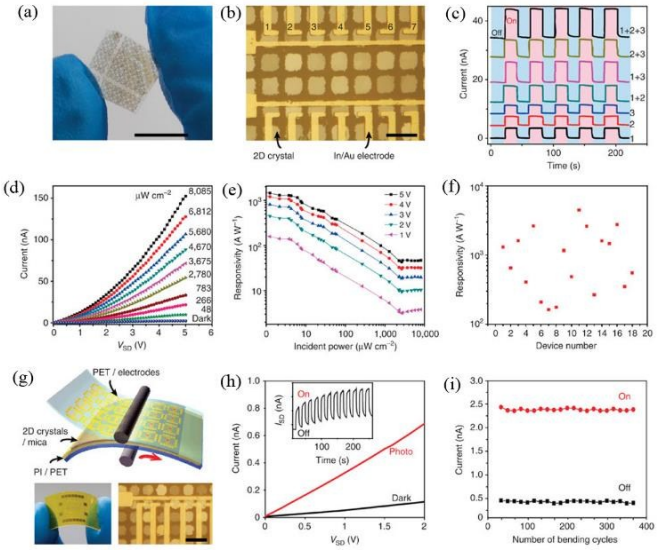

Fig. 11 Patterning 2D layered materials has a benefit for integration of electronic optoelectronic devices. (a) Photograph and (b) OM image of In_2Se_3 photodetector array. (c) photoresponse of In_2Se_3 photodetector. (d) IV curve in the dark and under different illuminations intensities. (e) Dependence of photoresponse on light intensities. (f) Statistic distribution of photoresponsivity of In_2Se_3 devices. (g) Schematic of device packaging. (h) Photoresponse characterization of the packaged device. (i) Current as a function of bending cycles. (Reproduced with permission from ref. 55. Copyright 2015 Macmillan Publishers Limited.)

4.3 Van der Waals heterostructures

Heterostructure is a core structure and functional unit in many electronic and optoelectronic devices, such as light emitting diodes, solar cells, tunneling transistors, and so on.[125, 136, 137] With the rise and development of 2D layered materials, some researchers began to focus on the study of vdW heterostructures based on 2D layered materials. Encouraged by the first heterostructure based on graphene/h-BN proposed by Dean et al. in 2010,[126] various other similar works have been reported.[125, 136, 137, 139, 140] The initial concept about vdW heterostructures was put forward by Geim and Grigorieva in 2013.[141] This artificial heterostructure is comprised of different 2D layered materials stacked together in a chosen sequence. Each isolated 2D layered material could be considered as

building blocks, which are connected to each other through weak vdW force. Therefore, different from conventional 3D heterostructures, vdW heterostructures can circumvent strict requirement of lattice matching. The very easy requirement on crystal structure matching coupled with the unique natures of various 2D layered materials enables to controllably synthesize vdW heterostructures with novel properties. To begin with we will introduce how to build a vdW heterostructure which is a base to realize their fascinating applications.

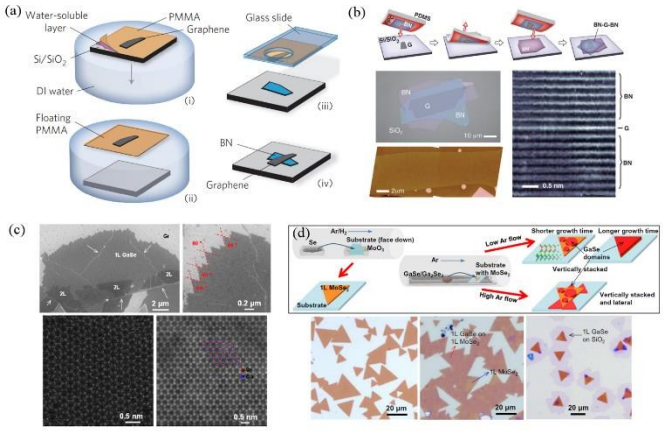

Fig. 12 Fabrication of vdW heterostructures by mechanical transfer and CVD methods. (a) Schematic illustrating the transfer process utilized to build graphene/h-BN heterostructures. (Reproduced with permission from ref. 138. Copyright 2010 Macmillan Publishers Limited.) (b) Schematic illustrating the assembly procedure without using liquid. Bottom panel: optical, AFM, and high-resolution cross section ADF-STEM image of BN/graphene/BN heterostructures. (Reproduced with permission from ref. 142. Copyright 2013 the American Association for the Advancement of Science.) (c) Top panel: SEM images of GaSe epilayer on graphene. Bottom panel: ADF-STEM images of 1L graphene and 1L vdW epitaxial GaSe on graphene. (Reproduced with permission from ref. 77. Copyright 2015 American Chemical Society.) (d) The experimental setting for the growth and optical micrographs of 1L $MoSe_2$ and GaSe/$MoSe_2$ heterostructures. (Reproduced with permission from ref. 145. Copyright 2016 the American Association for the Advancement of Science.)

In general, there are two methods to fabricate vdW heterostructures. One approach is mechanical transfer. A typical transfer process was originally realized by Dean et al. in 2010, as illustrated in figure 12a. First of all, the desired layered material was exfoliated onto a polymer stack comprised of a water-soluble layer and a PMMA film. Subsequently the water-soluble layer and the PMMA film with the desired 2D layered building block were separated by soaking them in deionized water. The layered material to be transferred is precisely controlled by micro manipulator and reversely coated by the aimed building block at last. However, an immersion process was inevitable in this method, which was not good to get a clean interface. Therefore, a new assembly procedure without using liquid was developed to fabricate BN/graphene/BN heterostructures by Wang et al. in 2013,[142] as shown in figure 12b. In brief, one of 2D layered materials was used as a stamp to pick up another building block by vdW interaction in this way. Generally, both of the mechanical transfer process mentioned above just need simple facilities, which are facile and also vastly used to assemble vdW heterostructures based on group III–VI compounds.[143, 144] Nevertheless, this mechanical transfer method still has some deficiencies. The relatively low yield make it difficult to realize the volume production of devices. Moreover, it is difficult to precisely control stacking orientation and could introduce undesired impurities that are detrimental to device performance. In contrast, another method of in situ growth can conquer these issues very well and have been attracting more and more attentions.[77, 145-149] Li et al. reported growth of GaSe/graphene heterostructures through CVD method.[77] Figure 12c depicts SEM image of GaSe epilayer on graphene and atomic resolution aberration-corrected dark-field (ADF)-STEM images of 1L graphene and 1L vdW epitaxial GaSe on graphene. Very recently, Li et al. demonstrated synthesis of vertically stacked and lateral GaSe/$MoSe_2$ heterostructures via the same epitaxial technique.[145] Schematic of growth and optical micrograph of 1L $MoSe_2$ and GaSe/$MoSe_2$ heterostructures are illustrated in figure 12d. The bilayer heterostructrures consisting of monolayered GaSe/$MoSe_2$ exhibit atomically sharp interfaces and well-defined. In addition, molecular beam epitaxy (MBE) is also a common and effective growth technique. Moreover, it can exactly control the thickness of films with wafer-scale homogeneity and achieve scalable product of devices. For example, Yuan et al. and Liu et al. reported the controllable synthesis of GaSe and $GaTe_xSe_{1-x}$ on Si by molecular beam epitaxy, respectively.[148, 149] These growth processes based on vdW epitaxy can allow heteroepitaxy between various layered materials with large mismatches of lattice constants, as discussed in synthesis part. More importantly, these direct growth approaches can provide more clean, sharp and seamless stacking interface. Constructing vdW heterostructures based on group III–VI compounds by mechanical transfer and CVD, provides a new route toward exploring the electronic and optoelectronic properties.

Although vdW heterostructures based on intensively investigated 2D layered materials, such as graphene, h-BN, and TMDs, have been widely reported, adequate reports on heterostructures based on group III–VI compounds are still expected. Now we discuss and evaluate properties and applications of vdW heterostructures based on group III–VI compounds. As is well known, p-n junction underlies a large number of electronic and optoelectronic devices. When p- and n-type semiconductors are contacted together, holes in p-region and electrons in n-region can diffuse and recombine with each other. Then, there will be a depletion region in which the same amount of positive and negative charges are left at the interface. Meanwhile, build-in electric field is formed to prevent free carriers from diffusing. Eventually, both the drift and diffusion motions from build-in electric field and concentration gradient respectively can reach dynamic equilibrium. When p-n junction is forward biased, the barrier at the interface can be lower, resulting in a substantial electric current through p–n junctions. The case corresponds to on state of p-n junctions. Conversely, reverse bias can prevent significant electric current flow and turn it off state. This unidirectional transmission of current in p-n junctions is called rectification behavior. This unidirectional transmission of current in p-n junctions is called

rectification behavior which is the fundamental feature of p-n junction. Rectification feature is characterized by rectification ratio.

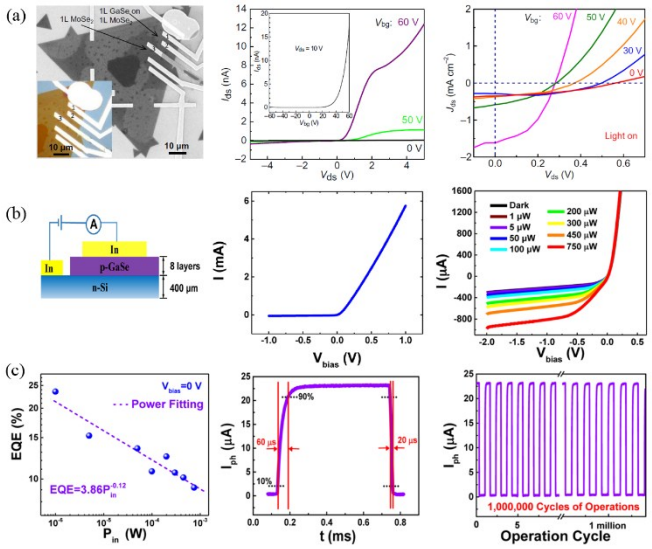

Fig. 13 Rectification feature, PV effect, and photoresponse of heterostructures based on group III–VI compounds. (a) SEM, AFM (inset) images, and gate-tunable rectification behavior and PV effect of GaSe/$MoSe_2$ heterostructures. (Reproduced with permission from ref. 145. Copyright 2016 the American Association for the Advancement of Science.) (b) Device model of a vertical GaSe/Si heterostructure and its rectification feature and PV effect changed with incidence laser power. (c) EQE under various laser powers at V_{bias} = 0 V, time-resolved photoresponse, and stability test of a 8-layer GaSe/Si diode. EQE is up to 23.6% and the fastest rise time can reach 60 μs. (b-c, reproduced with permission from ref. 148. Copyright 2015 American Chemical Society.)

Photovoltaic (PV) effect is another basic characteristic of p-n junctions. It refers to the generation of potential difference in p-n junctions under light illumination. If a p-n junction is connected to a loop, the separation of the photo-excited electron-hole pairs owing to the drive of build-in electric field can produce current in the circuit. On the basis of PV effect, solar cell is one of the most important optoelectronic applications of heterostructures. Their performance indicators include open-circuit voltage (V_{oc}), short-circuit current (I_{sc}), fill factor (FF), and conversion efficiency (η). Open-circuit voltage is the difference of electrical potentials between the two terminals of a solar cell when it is disconnected. Short-circuit current stands for the electric current flowing through a p–n junction when bias voltage is equal to 0 V. From current–voltage (I-V) curve, both of the parameters can be extracted. Fill factor and conversion efficiency are defined by $FF= I_mV_m/I_{sc}V_{oc}$ and $\eta = P_m/P_{in}$ respectively, where I_m and V_m are the current and voltage corresponding to maximal output power ($P_m= I_mV_m$), P_{in} is the incident power. As for vdW heterostructures based on group III–VI materials, they exhibit superior rectification characteristic and PV effect. For example, as shown in figure 13a, Li et al. demonstrated GaSe/$MoSe_2$ heterostructures with gate-tunable rectification behavior and PV effect.[145] At V_{bg} = 0 V, their open-circuit voltage, short-circuit current density, fill factor, and conversion efficiency are about 0.57 V, 0.35 mA/cm^2, 0.12%, and 0.38 respectively. Similarly, Yuan et al. fabricated vertical GaSe/Si p-n diodes,[148] which show a rectification ratio over 100 at 300 K. When temperature decreases to 120 K, the rectification ratio increases to10^5. The pronounced PV effect has also been found under various incident laser powers (figure 13b). In addition, as photodetectors, the vertical GaSe/Si heterostructures exhibit a high external quantum efficiency (EQE) of 23.6%, fast response time of 60 μs and steady photo-switching behavior after 1 million cycles of operation, as depicted in figure 13c.

Besides the applications based on p-n junctions mentioned above, hybridizing III–VI layered semiconductors with graphene to enhance optoelectronic performance have also been drawing increasing attentions.[143, 144, 150] It is generally known that graphene possesses ultrahigh mobility allowing fast transport of carriers and weak absorbance required by an optical window. As an appealing aspect, the work function of graphene is easily adjusted by external electric field to form the favorable band alignment between graphene and channel materials. Therefore, it is seen as a preferred candidate for use as transparent electrical contacts. For example, Mudd et al. reported a planar and vertical vdW graphene/InSe heterostructures in which graphene is used as electrodes.[143] Compared to Au-contacts, the disappearance of Schottky barrier at the interface and high conductivity of graphene significantly enhance photoresponsivity of InSe-based photodetectors, as shown in figure 14a. In their vertical counterparts (figure 14b), the channel length depends on the thickness of InSe nanosheet. The decreased distance between both of the graphene electrodes gives rise to the shortening of carrier transit time, and producing more sensitive photoresponse. The photoresponsivity can be observed up to 10^5 A/W at λ = 633 nm in this vertical heterostructures.

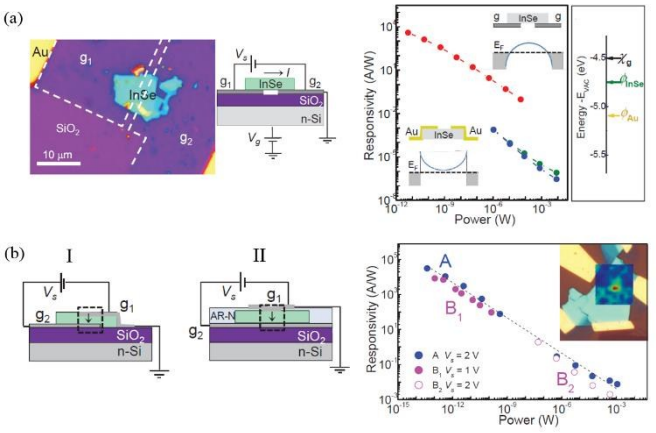

Fig. 14 (a) Schematic representation of planar van der Waals graphene/InSe heterostructures, in which graphene is used as electrodes. Right panel: photoresponsivity, band alignment of graphene/InSe/graphene and Au/InSe/Au heterostructures, as well as their work functions. (b) Schematic structures of two kinds of vertical graphene/InSe/graphene devices (type I and type II) and the photoresponsivity corresponded to type I (blue) and type II (magenta). T = 300 K, λ = 633 nm, V_s = 2 V, and V_g = 0 V. (Reproduced with permission from ref. 143. Copyright 2015 John Wiley & Sons, Inc.)

In another kind of graphene/InSe heterostructures demonstrated by Chen et al.,[144] the monolayer graphene covers

ultrathin InSe flake. Then, source/drain electrodes are deposited on graphene, as illustrated in figure 15a. Hence, the tight cover of graphene makes the ultrathin InSe flake to be stable in air. Moreover, graphene plays an important role in transporting photo-excited electrons. Figure 15b gives the corresponding band structure diagram of a graphene/InSe heterostructure at different gate voltages. Under illumination with a 532 nm laser, photo-excited electron-hole pairs are generated in InSe flake. Subsequently photo-excited electrons are effectively transferred to graphene and at the same time photo-excited holes remains in InSe due to the vertical architecture and electronic structure at the interface. Compared to separate InSe-based photodetector, graphene/InSe photodetector exhibits much excellent performance in photoresponsivity and external quantum efficiency, as displayed in figure 15c. Similar work has also been reported by Lu el at., wherein they demonstrated granphene/GaSe heterostructures with a high gain exceeding 10^7 and a fast response time of 10 ms.[150]

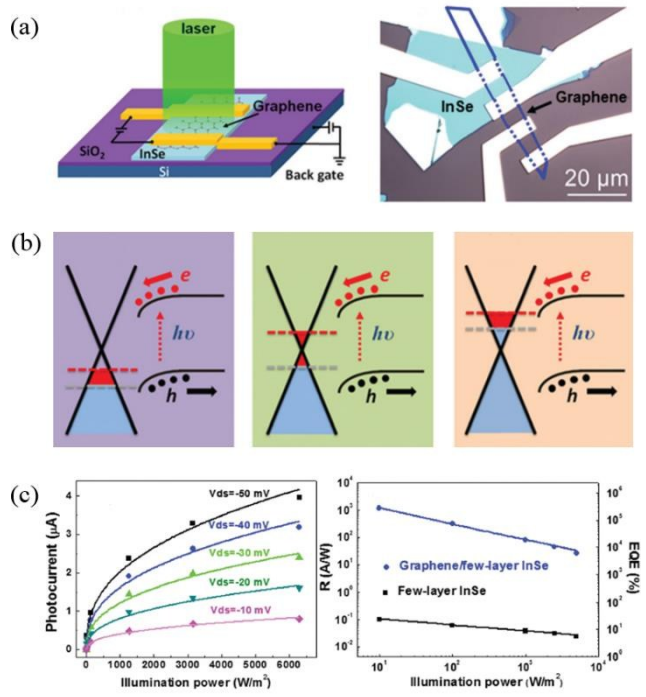

Fig. 15 Photodetector based on graphene/InSe heterostructures. (a) Schematic diagram and optical image of the device. Reproduced with permission. (b) The corresponding band structure diagram of a graphene/InSe heterostructure at different gate voltages. (c) Photocurrent, photoresponsivity, and EQE of the device changed with incident laser power ranging between 12.6 Wm^{-2} and 6.3 × 10^3 Wm^{-2}. The maximal photoresponsivity of 0.94 × 10^3 AW^{-1} and EQE of 2.18 × 10^5% are acquired at P = 12.6 Wm^{-2}, λ = 532 nm, V_{ds} = -50 mV, and V_g = 0 V. (Reproduced with permission from ref. 144. Copyright 2015 The Royal Society of Chemistry.)

5. Conclusions

Group III-VI compounds $M^{III}X^{VI}$ (M = Ga, In; X = S, Se, Te) are relatively new and exciting class of 2D layered materials possessing many superior properties that are not seen in TMDs family. We summarized the progress in the controlled synthesis and electronic and optoelectronic properties of 2D layered $M^{III}X^{VI}$ materials. Following the rise of new exciting opportunity, future electronic devices require advances in the synthesis of 2D layered $M^{III}X^{VI}$ materials. Although CVD and vdW epitaxy in 2D layered $M^{III}X^{VI}$ materials has been realized, large-scale, continuous, uniform and control-thickness thin films still need to be grown. Now, single-crystal graphene with several millimeter were synthesized. The preparation to monolayer $M^{III}X^{VI}$ without the presence of domain boundary and dislocation is required. The difficulty in synthesizing such films is uncontrollable nucleation sites. Thus, researchers may consider improving equipment of vapor-phase growth to realize controllable, stable and efficient precursors supply. In addition, low temperature growth techniques such as MBE and atomic layer deposition, may be given due attention. Wet chemistry synthesis is well developed with its simplicity and prolificacy. However, thickness of the products are usually uncontrollable. Because of different-thickness layered materials with different properties, large applications in the future depend on the improvement of wet chemistry methods. Further development of liquid phase method has a great benefit for the application of printed and flexible electronics on the market. On the other hand, the realization of integrating these layered materials needs the development of several techniques, such as reliable synthesis, contact engineering, selective doping, high-k dielectric deposition and so on, which require to be solved in the next few years. The chemical passivation and encapsulation of the 2D layered $M^{III}X^{VI}$ materials can further improve the carrier mobility. Combining vapor-phase synthesis with device integration may be an important breakout in the future. The properties and applications of 2D layered $M^{III}X^{VI}$ materials are exciting, expanding area of research and also extending to practical applications.

Acknowledgements

This work was supported by the National Natural Science Foundation of China (Nos. 21373065 and 61474033), 973 Program of the Ministry of Science and Technology of China (No. 2012CB934103), Beijing Natural Science Foundation (No. 2144059) and CAS Key Laboratory of Nanosystem and Hierarchical Fabrication. The authors gratefully acknowledge the support of Youth Innovation Promotion Association CAS.

Notes and references

1 A. K. Geim and K. S. Novoselov, *Nat. Mater.*, 2007, **6**, 183-191.
2 A. H. Castro Neto, F. Guinea, N. M. R. Peres, K. S. Novoselov and A. K. Geim, *Rev. Mod. Phys.*, 2009, **81**, 109-162.
3 B. Radisavljevic, A. Radenovic, J. Brivio, V. Giacometti and A. Kis, *Nat. Nanotechnol.*, 2011, **6**, 147-150.
4 K. F. Mak, C. Lee, J. Hone, J. Shan and T. F. Heinz, *Phys. Rev. Lett.*, 2010, **105**, 136805.
5 H. Fang, S. Chuang, T. C. Chang, K. Takei, T. Takahashi and A. Javey, *Nano Lett.*, 2012, **12**, 3788-3792.
6 K. Xu, Z. X. Wang, X. L. Du, M. Safdar, C. Jiang and J. He, *Nanotechnology*, 2013, **24**, 465705.

7 K. S. Kim, Y. Zhao, H. Jang, S. Y. Lee, J. M. Kim, K. S. Kim, J. H. Ahn, P. Kim, J. Y. Choi and B. H. Hong, *Nature*, 2009, **457**, 706-710.
8 K. Xu, F. M. Wang, Z. X. Wang, X. Y. Zhan, Q. S. Wang, Z. Z. Cheng, M. Safdar and J. He, *ACS Nano*, 2014, **8**, 8468-8476.
9 C. Tan and H. Zhang, *Nat. Commun.* 2015, **6**, 7873.
10 H. Zhang, *ACS Nano*, 2015, **9**, 9451-9469.
11 C. Tan and H. Zhang, *J. Am. Chem. Soc.*, 2015, **137**, 12162-12174.
12 Q. Liu, Y. Yu, Q. Ma, B. Chen and H. Zhang, *Adv. Mater.*, 2016, **28**, 1917-1933.
13 C. Tan and H. Zhang, *Chem. Soc. Rev.*, 2015, **44**, 2713-2731.
14 X. Huang, C. Tan, Z. Yin and H. Zhang, *Adv. Mater.*, 2014, **26**, 2185-2204.
15 A. K. Geim, *Science*, 2009, **324**, 1530-1534.
16 X. S. Li, W. W. Cai, J. H. An, S. Kim, J. Nah, D. X. Yang, R. Piner, A. Velamakanni, I. Jung, E. Tutuc, S. K. Banerjee, L. Colombo and R. S. Ruoff, *Science*, 2009, **324**, 1312-1314.
17 A. Reina, X. T. Jia, J. Ho, D. Nezich, H. B. Son, V. Bulovic, M. S. Dresselhaus and J. Kong, *Nano Lett.*, 2009, **9**, 30-35.
18 A. C. Ferrari, J. C. Meyer, V. Scardaci, C. Casiraghi, M. Lazzeri, F. Mauri, S. Piscanec, D. Jiang, K. S. Novoselov, S. Roth and A. K. Geim, *Phys. Rev. Lett.*, 2006, **97**, 187401.
19 Y. W. Son, M. L. Cohen and S. G. Louie, *Phys. Rev. Lett.*, 2006, **97**, 216803.
20 H. Li, J. Wu, Z. Yin and H. Zhang, *Acc. Chem. Res.*, 2014, **47**, 1067-1075.
21 K. S. Novoselov, A. K. Geim, S. V. Morozov, D. Jiang, M. I. Katsnelson, I. V. Grigorieva, S. V. Dubonos and A. A. Firsov, *Nature*, 2005, **438**, 197-200.
22 A. A. Balandin, S. Ghosh, W. Z. Bao, I. Calizo, D. Teweldebrhan, F. Miao and C. N. Lau, *Nano Lett.*, 2008, **8**, 902-907.
23 K. I. Bolotin, K. J. Sikes, Z. Jiang, M. Klima, G. Fudenberg, J. Hone, P. Kim and H. L. Stormer, *Solid State Commun.*, 2008, **146**, 351-355.
24 Y. W. Zhu, S. Murali, W. W. Cai, X. S. Li, J. W. Suk, J. R. Potts and R. S. Ruoff, *Adv. Mater.*, 2010, **22**, 3906-3924.
25 X. L. Li, X. R. Wang, L. Zhang, S. W. Lee and H. J. Dai, *Science*, 2008, **319**, 1229-1232.
26 W. Cao, J. H. Kang, D. Sarkar, W. Liu and K. Banerjee, *IEEE Trans. Electron Devices*, 2015, **62**, 3459-3469.
27 W. J. Yu, Y. Liu, H. L. Zhou, A. X. Yin, Z. Li, Y. Huang and X. F. Duan, *Nat. Nanotechnol.*, 2013, **8**, 952-958.
28 G. Eda, T. Fujita, H. Yamaguchi, D. Voiry, M. W. Chen and M. Chhowalla, *ACS Nano*, 2012, **6**, 7311-7317.
29 W. J. Yu, Z. Li, H. L. Zhou, Y. Chen, Y. Wang, Y. Huang and X. F. Duan, *Nat. Mater.*, 2013, **12**, 246-252.
30 G. Eda, H. Yamaguchi, D. Voiry, T. Fujita, M. W. Chen and M. Chhowalla, *Nano Lett.*, 2011, **11**, 5111-5116.
31 H. L. Zeng, J. F. Dai, W. Yao, D. Xiao and X. D. Cui, *Nat. Nanotechnol.*, 2012, **7**, 490-493.
32 D. Xiao, G. B. Liu, W. X. Feng, X. D. Xu and W. Yao, *Phys. Rev. Lett.*, 2012, **108**, 196802.
33 J. Kibsgaard, Z. B. Chen, B. N. Reinecke and T. F. Jaramillo, *Nat. Mater.*, 2012, **11**, 963-969.
34 Y. Feldman, E. Wasserman, D. J. Srolovitz and R. Tenne, *Science*, 1995, **267**, 222-225.
35 P. Joensen, R. F. Frindt and S. R. Morrison, *Mater. Res. Bull.*, 1986, **21**, 457-461.
36 X. Huang, Z. Zeng and H. Zhang, *Chem. Soc. Rev.*, 2013, **42**, 1934-1946.
37 Y. Chen, C. Tan, H. Zhang and L. Wang, *Chem. Soc. Rev.*, 2015, **44**, 2681-2701.
38 C. Tan, Z. Liu, W. Huang and H. Zhang, *Chem. Soc. Rev.*, 2015, **44**, 2615-2628.
39 L. Luo, L. Chatzakis, J. Wang, F. B. P. Niesier, M. Wegener, T. Koschny and C. M. Soukoulis, *Nat. Commun.* 2013, **4**, 3055.
40 W. Jie, X. Chen, D. Li, Y. Y. Hui, S. P. Lau, X. Cui and J. Hao, Angew. Chem. Int. Edit., 2015, **54**, 1185-1189.
41 W. J. Zhao, Z. Ghorannevis, L. Q. Chu, M. L. Toh, C. Kloc, P. H. Tan and G. Eda, *ACS Nano*, 2013, **7**, 791-797.
42 W. Liu, J. Kang, W. Cao, D. Sarkar, Y. Khatami, D. Jena and K. Banerjee, *IEEE International Electron Devices Meeting*, 2013, 19.4.1 - 19.4.4.
43 W. Liu, D. Sarkar, J. H. Kang, W. Cao and K. Banerjee, *ACS Nano*, 2015, **9**, 7904-7912.
44 K. Kang, S. E. Xie, L. J. Huang, Y. M. Han, P. Y. Huang, K. F. Mak, C. J. Kim, D. Muller and J. Park, *Nature*, 2015, **520**, 656-660.
45 D. Sarkar, X. J. Xie, J. H. Kang, H. J. Zhang, W. Liu, J. Navarrete, M. Moskovits and K. Banerjee, *Nano Lett.*, 2015, **15**, 2852-2862.
46 O. Lopez-Sanchez, D. Lembke, M. Kayci, A. Radenovic and A. Kis, *Nat. Nanotechnol.*, 2013, **8**, 497-501.
47 D. J. Late, B. Liu, J. J. Luo, A. M. Yan, H. S. S. R. Matte, M. Grayson, C. N. R. Rao and V. P. Dravid, *Adv. Mater.*, 2012, **24**, 3549-3554.
48 P. A. Hu, L. F. Wang, M. Yoon, J. Zhang, W. Feng, X. N. Wang, Z. Z. Wen, J. C. Idrobo, Y. Miyamoto, D. B. Geohegan and K. Xiao, *Nano Lett.*, 2013, **13**, 1649-1654.
49 P. A. Hu, Z. Z. Wen, L. F. Wang, P. H. Tan and K. Xiao, *ACS Nano*, 2012, **6**, 5988-5994.
50 W. Wei, Y. Dai, C. W. Niu, X. Li, Y. D. Ma and B. B. Huang, *J. Mater. Chem. C*, 2015, **3**, 11548-11554.
51 Z. X. Wang, K. Xu, Y. C. Li, X. Y. Zhan, M. Safdar, Q. S. Wang, F. M. Wang and J. He, *ACS Nano*, 2014, **8**, 4859-4865.
52 P. G. Hu, J. Zhang, M. N. Yoon, X. F. Qiao, X. Zhang, W. Feng, P. H. Tan, W. Zheng, J. J. Liu, X. N. Wang, J. C. Idrobo, D. B. Geohegan and K. Xiao, *Nano Res.*, 2014, **7**, 694-703.
53 X. Tao, E. Mafi and Y. Gu, *Appl. Phys. Lett.*, 2013, **103**, 193115.
54 D. Wu, A. J. Pak, Y. N. Liu, Y. Zhou, X. Y. Wu, Y. H. Zhu, M. Lin, Y. Han, Y. Ren, H. L. Peng, Y. H. Tsai, G. S. Hwang and K. J. Lai, *Nano Lett.*, 2015, **15**, 8136-8140.
55 W. S. Zheng, T. Xie, Y. Zhou, Y. L. Chen, W. Jiang, S. L. Zhao, J. X. Wu, Y. M. Jing, Y. Wu, G. C. Chen, Y. F. Guo, J. B. Yin, S. Y. Huang, H. Q. Xu, Z. F. Liu and H. L. Peng, *Nat. Commun.*, 2015, **6**, 6972.
56 S. Sucharitakul, N. J. Goble, U. R. Kumar, R. Sankar, Z. A. Bogorad, F. C. Chou, Y. T. Chen and X. P. A. Gao, *Nano Lett.*, 2015, **15**, 3815-3819.
57 M. Mahjouri-Samani, R. Gresback, M. K. Tian, K. Wang, A. A. Puretzky, C. M. Rouleau, G. Eres, I. N. Ivanov, K. Xiao, M. A. McGuire, G. Duscher and D. B. Geohegan, *Adv. Funct. Mater.*, 2014, **24**, 6365-6371.
58 W. Feng, W. Zheng, W. W. Cao and P. A. Hu, *Adv. Mater.*, 2014, **26**, 6587-6593.
59 S. R. Tamalampudi, Y. Y. Lu, U. R. Kumar, R. Sankar, C. D. Liao, B. K. Moorthy, C. H. Cheng, F. C. Chou and Y. T. Chen, *Nano Lett.*, 2014, **14**, 2800-2806.
60 W. Feng, J. B. Wu, X. L. Li, W. Zheng, X. Zhou, K. Xiao, W. W. Cao, B. Yang, J. C. Idrobo, L. Basile, W. Q. Tian, P. H. Tan and P. A. Hu, *J. Mater. Chem. C*, 2015, **3**, 7022-7028.
61 P. Gomes da Costa, R. G. Dandrea, R. F. Wallis and M. Balkanski, *Phys. Rev. B*, 1993, **48**, 14135-14141.
62 S. D. Lei, L. H. Ge, S. Najmaei, A. George, R. Kappera, J. Lou, M. Chhowalla, H. Yamaguchi, G. Gupta, R. Vajtai, A. D. Mohite and P. M. Ajayan, *ACS Nano*, 2014, **8**, 1263-1272.
63 G. W. Mudd, S. A. Svatek, T. Ren, A. Patane, O. Makarovsky, L. Eaves, P. H. Beton, Z. D. Kovalyuk, G. V. Lashkarev, Z. R. Kudrynskyi and A. I. Dmitriev, *Adv. Mater*, 2013, **25**, 5714-5718.
64 D. J. Late, B. Liu, H. S. S. R. Matte, C. N. R. Rao and V. P. Dravid, *Adv. Funct. Mater.*, 2012, **22**, 1894-1905.
65 S. D. Lei, L. H. Ge, Z. Liu, S. Najmaei, G. Shi, G. You, J. Lou, R. Vajtai and P. M. Ajayan, *Nano Lett.*, 2013, **13**, 2777-2781.

66 D. V. Rybkovskiy, A. V. Osadchy and E. D. Obraztsova, *Phys. Rev. B*, 2014, **90**, 235302.
67 A. Yamamoto, A. Syouji, T. Goto, E. Kulatov, K. Ohno, Y. Kawazoe, K. Uchida and N. Miura, *Phys. Rev. B*, 2001, **64**, 035210.
68 X. H. Yu, T. J. Hou, X. H. Sun and Y. Y. Li, *Solid State Commun.*, 2013, **162**, 28-33.
69 J. D. Zhou, Q. S. Zeng, D. H. Lv, L. F. Sun, L. Niu, W. Fu, F. C. Liu, Z. X. Shen, C. H. Jin and Z. Liu, *Nano Lett.*, 2015, **15**, 6400-6405.
70 X. Tao and Y. Gu, *Nano Lett.*, 2013, **13**, 3501-3505.
71 S. Marsillac, A. M. CombotMarie, J. C. Bernede and A. Conan, *Thin Solid Films*, 1996, **288**, 14-20.
72 B. Yu, S. Y. Ju, X. H. Sun, G. Ng, T. D. Nguyen, M. Meyyappan and D. B. Janes, *Appl. Phys. Lett.*, 2007, **91**, 133119.
73 M. Ishikawa and T. Nakayama, *Jpn. J. Appl. Phys.*, 1997, **36**, L1576-L1579.
74 G. Yu, Z. Liu, X. M. Xie, X. Ouyang and G. Z. Shen, *J. Mater. Chem. C*, 2014, **2**, 6104-6110.
75 Z. X. Wang, M. Safdar, M. Mirza, K. Xu, Q. S. Wang, Y. Huang, F. M. Wang, X. Y. Zhan and J. He, *Nanoscale*, 2015, **7**, 7252-7258.
76 M. Lin, D. Wu, Y. Zhou, W. Huang, W. Jiang, W. S. Zheng, S. L. Zhao, C. H. Jin, Y. F. Guo, H. L. Peng and Z. F. Liu, *J. Am. Chem. Soc.*, 2013, **135**, 13274-13277.
77 X. F. Li, L. Basile, B. Huang, C. Ma, J. W. Lee, I. V. Vlassiouk, A. A. Puretzky, M. W. Lin, M. Yoon, M. F. Chi, J. C. Idrobo, C. M. Rouleau, B. G. Sumpter, D. B. Geohegan and K. Xiao, *ACS Nano*, 2015, **9**, 8078-8088.
78 X. Zhou, J. X. Cheng, Y. B. Zhou, T. Cao, H. Hong, Z. M. Liao, S. W. Wu, H. L. Peng, K. H. Liu and D. P. Yu, *J. Am. Chem. Soc.*, 2015, **137**, 7994-7997.
79 Z. X. Wang, M. Safdar, C. Jiang and J. He, *Nano Lett.*, 2012, **12**, 4715-4721.
80 T. R. Wu, X. F. Zhang, Q. H. Yuan, J. C. Xue, G. Y. Lu, Z. H. Liu, H. S. Wang, H. M. Wang, F. Ding, Q. K. Yu, X. M. Xie and M. H. Jiang, *Nat. Mater.*, 2016, **15**, 43-47.
81 D. F. Liu, W. H. Zhang, D. X. Mou, J. F. He, Y. B. Ou, Q. Y. Wang, Z. Li, L. L. Wang, L. Zhao, S. L. He, Y. Y. Peng, X. Liu, C. Y. Chen, L. Yu, G. D. Liu, X. L. Dong, J. Zhang, C. T. Chen, Z. Y. Xu, J. P. Hu, X. Chen, X. C. Ma, Q. K. Xue and X. J. Zhou, *Nat. Commun.*, 2012, **3**, 931.
82 A. L. Briseno, S. C. B. Mannsfeld, M. M. Ling, S. H. Liu, R. J. Tseng, C. Reese, M. E. Roberts, Y. Yang, F. Wudl and Z. N. Bao, *Nature*, 2006, **444**, 913-917.
83 J. Aizenberg, A. J. Black and G. M. Whitesides, *Nature*, 1999, **398**, 495-498.
84 H. Minemawari, T. Yamada, H. Matsui, J. Tsutsumi, S. Haas, R. Chiba, R. Kumai and T. Hasegawa, *Nature*, 2011, **475**, 364-367.
85 Y. B. Zhou, Y. F. Nie, Y. J. Liu, K. Yan, J. H. Hong, C. H. Jin, Y. Zhou, J. B. Yin, Z. F. Liu and H. L. Peng, *ACS Nano*, 2014, **8**, 1485-1490.
86 Y. N. Xia and G. M. Whitesides, *Angew. Chem.-Int. Edit.*, 1998, **37**, 550-575.
87 T. Ahamad and S. M. Alshehri, *Nano Hybrids*, 2014, **6,** 37-46.
88 A. Harvey, C. Backes, Z. Gholamvand, D. Hanlon, D. McAteer, H. C. Nerl, E. McGuire, A. Seral-Ascaso, Q. M. Ramasse, N. McEvoy, S. Winters, N. C. Berner, D. McCloskey, J. F. Donegan, G. S. Duesberg, V. Nicolosi and J. N. Coleman, *Chem. Mat.*, 2015, **27**, 3483-3493.
89 O. I. Aksimentyeva, P. Y. Demchenko, V. P. Savchyn and O. A. Balitskii, *Nanoscale Res. Lett.*, 2013, **8**, 29.
90 J. Lauth, F. E. S. Gorris, M. S. Khoshkhoo, T. Chasse, W. Friedrich, V. Lebedeya, A. Meyer, C. Klinke, A. Komowsld, M. Scheele and H. Weller, *Chem. Mat.*, 2016, **28**, 1728-1736.
91 A. Seral-Ascaso, S. Metel, A. Pokle, C. Backes, C. J. Zhang, H. C. Nerl, K. Rode, N. C. Berner, C. Downing, N. McEvoy, E. Munoz, A. Harvey, Z. Gholamvand, G. S. Duesberg, J. N. Coleman and V. Nicolosi, *Nanoscale*, 2016, **8**, 11698-11706.
92 Q. H. Wang, K. Kalantar-Zadeh, A. Kis, J. N. Coleman and M. S. Strano, *Nat. Nanotechnol.*, 2012, **7**, 699-712.
93 J. S. Son, X. D. Wen, J. Joo, J. Chae, S. I. Baek, K. Park, J. H. Kim, K. An, J. H. Yu, S. G. Kwon, S. H. Choi, Z. W. Wang, Y. W. Kim, Y. Kuk, R. Hoffmann and T. Hyeon, Angew. Chem. Int. Edit., 2009, **48**, 6861-6864.
94 J. S. Son, J. H. Yu, S. G. Kwon, J. Lee, J. Joo and T. Hyeon, *Adv. Mater.*, 2011, **23**, 3214-3219.
95 J. Joo, J. S. Son, S. G. Kwon, J. H. Yu and T. Hyeon, *J. Am. Chem. Soc.*, 2006, **128**, 5632-5633.
96 X. Meng, J. A. Libera, T. T. Fister, H. Zhou, J. K. Hedlund, P. Fenter and J. W. Elam, *Chem. Mat.*, 2014, **26**, 1029-1039.
97 K. Cinar, Z. Caldiran, C. Coskun and S. Aydogan, *Thin Solid Films*, 2014, **550**, 40-45.
98 K. Mistry, C. Allen, C. Auth, B. Beattie, D. Bergstrom, M. Bost, M. Brazier, M. Buehler, A. Cappellani and R. Chau, *IEEE International Electron Devices Meeting*, 2007, 247 - 250.
99 W. Cao, J. Kang, D. Sarkar, W. Liu and K. Banerjee, *IEEE International Electron Devices Meeting*, 2014, 30.5.1 - 30.5.4.
100 B. Radisavljevic, M. B. Whitwick and A. Kis, *ACS Nano*, 2011, **5**, 9934-9938.
101 X. M. Zou, J. L. Wang, C. H. Chiu, Y. Wu, X. H. Xiao, C. Z. Jiang, W. W. Wu, L. Q. Mai, T. S. Chen, J. C. Li, J. C. Ho and L. Liao, *Adv. Mater.*, 2014, **26**, 6255-6261.
102 X. Ling, Y. H. Lee, Y. X. Lin, W. J. Fang, L. L. Yu, M. S. Dresselhaus and J. Kong, *Nano Lett.*, 2014, **14**, 464-472.
103 Y. J. Zhan, Z. Liu, S. Najmaei, P. M. Ajayan and J. Lou, *Small*, 2012, **8**, 966-971.
104 D. Sarkar, X. J. Xie, W. Liu, W. Cao, J. H. Kang, Y. J. Gong, S. Kraemer, P. M. Ajayan and K. Banerjee, *Nature*, 2015, **526**, 91-95.
105 Z. Y. Yin, H. Li, H. Li, L. Jiang, Y. M. Shi, Y. H. Sun, G. Lu, Q. Zhang, X. D. Chen and H. Zhang, *ACS Nano*, 2012, **6**, 74-80.
106 J. S. Ross, P. Klement, A. M. Jones, N. J. Ghimire, J. Q. Yan, D. G. Mandrus, T. Taniguchi, K. Watanabe, K. Kitamura, W. Yao, D. H. Cobden and X. D. Xu, *Nat. Nanotechnol.*, 2014, **9**, 268-272.
107 W. Liu, J. H. Kang, D. Sarkar, Y. Khatami, D. Jena and K. Banerjee, *Nano Lett.*, 2013, **13**, 1983-1990.
108 H. Wang, L. L. Yu, Y. H. Lee, Y. M. Shi, A. Hsu, M. L. Chin, L. J. Li, M. Dubey, J. Kong and T. Palacios, *Nano Lett.*, 2012, **12**, 4674-4680.
109 Y. Yoon, K. Ganapathi and S. Salahuddin, *Nano Lett*, 2011, **11**, 3768-3773.
110 A. Segura, F. Pomer, A. Cantarero, W. Krause and A. Chevy, *Phys. Rev. B*, 1984, **29**, 5708-5717.
111 P. I. Savitskii, Z. D. Kovalyuk and I. V. Mintyanskii, *Status Solidi A-Appl. Res.*, 2000, **180**, 523-531.
112 Z. H. Yu, Z. Y. Ong, Y. M. Pan, Y. Cui, R. Xin, Y. Shi, B. G. Wang, Y. Wu, T. S. Chen, Y. W. Zhang, G. Zhang and X. R. Wang, *Adv. Mater.*, 2016, **28**, 547-552.
113 B. Radisavljevic and A. Kis, *Nat. Mater.*, 2013, **12**, 815-820.
114 J. K. Huang, J. Pu, C. L. Hsu, M. H. Chiu, Z. Y. Juang, Y. H. Chang, W. H. Chang, Y. Iwasa, T. Takenobu and L. J. Li, *ACS Nano*, 2014, **8**, 923-930.
115 G. Fiori, F. Bonaccorso, G. Iannaccone, T. Palacios, D. Neumaier, A. Seabaugh, S. K. Banerjee and L. Colombo, *Nat. Nanotechnol.*, 2014, **9**, 768-779.
116 K. Xu, Y. Huang, B. Chen, Y. Xia, W. Lei, Z. Wang, Q. Wang, F. Wang, L. Yin and J. He, *Small*, 2016, **12**, 3106-3111.
117 J. O. Island, S. I. Blanter, M. Buscema, H. S. J. van der Zant and A. Castellanos-Gomez, *Nano Lett.*, 2015, **15**, 7853-7858.
118 Y. L. Cui, D. D. Caudel, P. Bhattacharya, A. Burger, K. C. Mandal, D. Johnstone and S. A. Payne, *J. Appl. Phys.*, 2009, **105**, 053709.
119 H. S. Lee, S. W. Min, Y. G. Chang, M. K. Park, T. Nam, H. Kim, J. H. Kim, S. Ryu and S. Im, *Nano Lett.*, 2012, **12**, 3695-3700.

120 K. Roy, M. Padmanabhan, S. Goswami, T. P. Sai, G. Ramalingam, S. Raghavan and A. Ghosh, *Nat. Nanotechnol.*, 2013, **8**, 826-830.
121 W. Choi, M. Y. Cho, A. Konar, J. H. Lee, G. B. Cha, S. C. Hong, S. Kim, J. Kim, D. Jena, J. Joo and S. Kim, *Adv. Mater.*, 2012, **24**, 5832-5836.
122 W. J. Zhang, C. P. Chuu, J. K. Huang, C. H. Chen, M. L. Tsai, Y. H. Chang, C. T. Liang, Y. Z. Chen, Y. L. Chueh, J. H. He, M. Y. Chou and L. J. Li, *Sci Rep*, 2014, **4**, 3826.
123 W. J. Zhang, J. K. Huang, C. H. Chen, Y. H. Chang, Y. J. Cheng and L. J. Li, *Adv. Mater.*, 2013, **25**, 3456-3461.
124 M. Buscema, M. Barkelid, V. Zwiller, H. S. J. van der Zant, G. A. Steele and A. Castellanos-Gomez, *Nano Lett.*, 2013, **13**, 358-363.
125 R. Cheng, D. H. Li, H. L. Zhou, C. Wang, A. X. Yin, S. Jiang, Y. Liu, Y. Chen, Y. Huang and X. F. Duan, *Nano Lett.*, 2014, **14**, 5590-5597.
126 L. Wang, J. S. Jie, Z. B. Shao, Q. Zhang, X. H. Zhang, Y. M. Wang, Z. Sun and S. T. Lee, *Adv. Funct. Mater.*, 2015, **25**, 2910-2919.
127 Z. H. Sun and H. X. Chang, *ACS Nano*, 2014, **8**, 4133-4156.
128 F. H. L. Koppens, T. Mueller, P. Avouris, A. C. Ferrari, M. S. Vitiello and M. Polini, *Nat. Nanotechnol.*, 2014, **9**, 780-793.
129 A. Splendiani, L. Sun, Y. B. Zhang, T. S. Li, J. Kim, C. Y. Chim, G. Galli and F. Wang, *Nano Lett.*, 2010, **10**, 1271-1275.
130 K. Xu, Z. X. Wang, F. Wang, Y. Huang, F. M. Wang, L. Yin, C. Jiang and J. He, *Adv. Mater.*, 2015, **27**, 7881-7887.
131 X. Gong, M. H. Tong, Y. J. Xia, W. Z. Cai, J. S. Moon, Y. Cao, G. Yu, C. L. Shieh, B. Nilsson and A. J. Heeger, *Science*, 2009, **325**, 1665-1667.
132 K. K. Manga, J. Z. Wang, M. Lin, J. Zhang, M. Nesladek, V. Nalla, W. Ji and K. P. Loh, *Adv. Mater.*, 2012, **24**, 1697-1702.
133 K. K. Manga, S. Wang, M. Jaiswal, Q. L. Bao and K. P. Loh, *Adv. Mater.*, 2010, **22**, 5265-5270.
134 S. D. Lei, F. F. Wen, L. H. Ge, S. Najmaei, A. George, Y. J. Gong, W. L. Gao, Z. H. Jin, B. Li, J. Lou, J. Kono, R. Vajtai, P. Ajayan and N. J. Halas, *Nano Lett.*, 2015, **15**, 3048-3055.
135 R. B. Jacobs-Gedrim, M. Shanmugam, N. Jain, C. A. Durcan, M. T. Murphy, T. M. Murray, R. J. Matyi, R. L. Moore and B. Yu, *ACS Nano*, 2014, **8**, 514-521.
136 R. S. Yan, S. Fathipour, Y. M. Han, B. Song, S. D. Xiao, M. D. Li, N. Ma, V. Protasenko, D. A. Muller, D. Jena and H. G. Xing, *Nano Lett.*, 2015, **15**, 5791-5798.
137 M. M. Furchi, A. Pospischil, F. Libisch, J. Burgdorfer and T. Mueller, *Nano Lett.*, 2014, **14**, 4785-4791.
138 C. R. Dean, A. F. Young, I. Meric, C. Lee, L. Wang, S. Sorgenfrei, K. Watanabe, T. Taniguchi, P. Kim, K. L. Shepard and J. Hone, *Nat. Nanotechnol.*, 2010, **5**, 722-726.
139 C. H. Lee, G. H. Lee, A. M. van der Zande, W. C. Chen, Y. L. Li, M. Y. Han, X. Cui, G. Arefe, C. Nuckolls, T. F. Heinz, J. Guo, J. Hone and P. Kim, *Nat. Nanotechnol.*, 2014, **9**, 676-681.
140 Y. X. Deng, Z. Luo, N. J. Conrad, H. Liu, Y. J. Gong, S. Najmaei, P. M. Ajayan, J. Lou, X. F. Xu and P. D. Ye, *ACS Nano*, 2014, **8**, 8292-8299.
141 A. K. Geim and I. V. Grigorieva, *Nature*, 2013, **499**, 419-425.
142 L. Wang, I. Meric, P. Y. Huang, Q. Gao, Y. Gao, H. Tran, T. Taniguchi, K. Watanabe, L. M. Campos, D. A. Muller, J. Guo, P. Kim, J. Hone, K. L. Shepard and C. R. Dean, *Science*, 2013, **342**, 614-617.
143 G. W. Mudd, S. A. Svatek, L. Hague, O. Makarovsky, Z. R. Kudrynskyi, C. J. Mellor, P. H. Beton, L. Eaves, K. S. Novoselov, Z. D. Kovalyuk, E. E. Vdovin, A. J. Marsden, N. R. Wilson and A. Patane, *Adv. Mater.*, 2015, **27**, 3760-3766.
144 Z. S. Chen, J. Biscaras and A. Shukla, *Nanoscale*, 2015, **7**, 5981-5986.
145 X. Li, M.-W. Lin, J. Lin, B. Huang, A. A. Puretzky, C. Ma, K. Wang, W. Zhou, S. T. Pantelides, M. Chi, I. Kravchenko, J. Fowlkes, C. M. Rouleau, D. B. Geohegan and K. Xiao, *Sci. Adv.*, 2016, **2**, e1501882.
146 Z. R. Kudrynskyi, A. P. Bakhtinov, V. N. Vodopyanov, Z. D. Kovalyuk, M. V. Tovarnitskii and O. S. Lytvyn, *Nanotechnology*, 2015, **26**, 465601.
147 K. C. Mandal and S. Das, *Photovoltaic Specialists Conference*, 2012, 000177 - 000180.
148 X. Yuan, L. Tang, S. S. Liu, P. Wang, Z. G. Chen, C. Zhang, Y. W. Liu, W. Y. Wang, Y. C. Zou, C. Liu, N. Guo, J. Zou, P. Zhou, W. D. Hu and F. X. Xiu, *Nano Lett.*, 2015, **15**, 3571-3577.
149 S. S. Liu, X. Yuan, P. Wang, Z. G. Chen, L. Tang, E. Z. Zhang, C. Zhang, Y. W. Liu, W. Y. Wang, C. Liu, C. Chen, J. Zou, W. D. Hu and F. X. Xiu, *ACS Nano*, 2015, **9**, 8592-8598.
150 R. T. Lu, J. W. Liu, H. F. Luo, V. Chikan and J. Z. Wu, *Sci Rep*, 2016, **6**, 19161.